AGU PUBLICATIONS

Water Resources Research

RESEARCH ARTICLE
10.1002/2016WR019722

Special Section:
Concentration-discharge Relations in the Critical Zone

Key Points:
- Controls on C-Q relationships were investigated based on simultaneous observations of both groundwater and stream water chemistry
- Rapid water chemistry evolution in the vadose zone and mineral equilibria in the saturated zone lead to stream's narrow concentration range
- Nonconservative transition from the subsurface to the surface may drive the C-Q relationships even more chemostatic for some elements

Supporting Information:
- Supporting Information S1

Correspondence to:
H. Kim,
hxk31@psu.edu

Citation:
Kim, H., W. E. Dietrich, B. M. Thurnhoffer, J. K. B. Bishop, and I. Y. Fung (2017), Controls on solute concentration-discharge relationships revealed by simultaneous hydrochemistry observations of hillslope runoff and stream flow: The importance of critical zone structure, *Water Resour. Res.*, *53*, doi:10.1002/2016WR019722.

Received 30 AUG 2016
Accepted 14 JAN 2017
Accepted article online 27 JAN 2017

Controls on solute concentration-discharge relationships revealed by simultaneous hydrochemistry observations of hillslope runoff and stream flow: The importance of critical zone structure

Hyojin Kim[1], William E. Dietrich[2], Benjamin M. Thurnhoffer[2], Jim K. B. Bishop[2,3], and Inez Y. Fung[2]

[1]Earth and Engineering Systems Institute, The Pennsylvania State University, University Park, Pennsylvania, USA, [2]Department of Earth and Planetary Science, University of California, Berkeley, California, USA, [3]Lawrence Berkeley National Laboratory, Berkeley, California, USA

Abstract We investigated controls on concentration-discharge relationships of a catchment underlain by argillite by monitoring both groundwater along a hillslope transect and stream chemistry. Samples were collected at 1–3 day intervals over 4 years (2009–2013) in Elder Creek in the Eel River Critical Zone Observatory in California. Runoff at our study hillslope is driven by vadose zone flux through deeply weathered argillite (5–25 m thick) to a perched, seasonally dynamic groundwater that then drains to Elder Creek. Low flow derives from the slowly draining deepest perched groundwater that reaches equilibrium between primary and secondary minerals and saturation with calcite under high subsurface pCO_2. Arriving winter rains pass through the thick vadose zone, where they rapidly acquire solutes via cation exchange reactions (driven by high pCO_2), and then recharge the groundwater that delivers runoff to the stream. These new waters displayed lower solute concentrations than the deep groundwater by less than a factor of 5 (except for Ca). Up to 74% of the total annual solute flux is derived from the vadose zone. The deep groundwater's Ca concentration decreased as it exfiltrates to the stream due to CO_2 degassing and this Ca loss is equivalent of 30% of the total chemical weathering flux of Elder Creek. The thick vadose zone in weathered bedrock and the perched groundwater on underlying fresh bedrock result in two distinct processes that lead to the relatively invariant (chemostatic) concentration-discharge behavior. The processes controlling solute chemistry are not evident from stream chemistry and runoff analysis alone.

1. Introduction

Rain and snow melt enters hillslopes introducing nearly negligible amounts of solutes but reaches adjacent streams having acquired solutes whose concentrations may be relatively time invariant (chemostatic) [e.g., *Bluth and Kump*, 1994; *White and Blum*, 1995; *Godsey et al*., 2009] or discharge dependent [e.g., *Shanley et al*., 2011; *Stallard and Murphy*, 2014]. In either case, the challenge is to understand what processes control the evolution of waters through the hillslope. This challenge has led research to focus on travel time distribution functions [e.g., *Kirchner et al*., 2001; *McGuire and McDonnell*, 2006; *Tetzlaff et al*., 2009; *Kirchner and Neal*, 2013; *Benettin et al*., 2015] and on the kinetic (e.g., reactive surface area, pCO_2, temperature, water-rock ratio) or thermodynamic controls along the travel paths [e.g., *Godsey et al*., 2009; *Clow and Mast*, 2010; *Maher*, 2011]. It is generally assumed that on hillslopes, solute evolution occurs primarily in the lateral groundwater runoff rather than the vertical passage through the vadose zone because hillslope lengths (~100 s of meters) are much longer than hillslope thicknesses (~10 s of meters) [*Kirchner et al*., 2001]. Models conceptualize subsurface compartments in the hillslope as composed of varying hydrologic and geochemical properties through which water advects, reacts, and possibly exchanges with prior chemically evolved water. [*Kirchner et al*., 2001; *Godsey et al*., 2009; *Maher*, 2011; *Benettin et al*., 2015]. The concentration-discharge (C-Q) relationships of elements in receiving streams are then treated as integral signals of these hillslope processes that can be used by models to constrain both reaction rates and equilibrium concentrations through multiple flow paths (or reservoirs) and thereby predict solute concentrations. The relative importance of these flow paths and geochemical controls will play out differently depending

on lithology, topography, and climate, and, in general, on the properties of the critical zone through which these processes transpire.

What are generally missing in these C-Q studies, however, are direct observations of the hydrologic and geochemical processes on the hillslopes contributing to runoff and an explicit, observationally based understanding of the critical zone structure that controls these processes: nearly all the studies have been developed exclusively upon stream chemistry observations [e.g., *Kirchner et al*., 2001; *Godsey et al*., 2009; *Maher*, 2011; *Kirchner and Neal*, 2013; *Benettin et al*., 2015]. Runoff generation processes at a hillslope scale have been extensively investigated in many catchments. One of the most commonly reported observations of these studies is a central role of vadose zone storage in runoff generation [e.g., *McDonnell*, 1990; *Montgomery et al*., 1997; *Sidle et al*., 2000; *Montgomery and Dietrich*, 2002; *Uchida et al*., 2005, 2006; *Tromp-van Meerveld and McDonnell*, 2006; *Salve et al*., 2012]. Once the rainfall input exceeds the vadose zone storage, runoff response becomes rapid and significant through various mechanisms typically involving preferential flow via macro-pores, fractures, and soil pipes [*Luxmoore et al*., 1990; *McDonnnell*, 1990; *Mulholland et al*., 1990; *Burns et al*., 1998; *Uchida et al*., 2005; *Tromp-van Meerveld and McDonnell*, 2006; *Salve et al*., 2012]. Elevated vadose zone moisture may also lead to pressure waves in response to pulses of rainfall [*Anderson et al*., 1997b; *Torres et al*., 1998]. As the infiltrated rainwater passes through the vadose zone, it undergoes chemical alteration. For example, sprinkler experiments carried out on a small, steep hillslope in Coos Bay, Oregon, USA, using both deionized and untreated stream water, reported that the hillslope runoff through the colluvial soil mantle displayed similar solute levels regardless of the input water's chemistry [*Anderson et al*., 1997a]. The authors proposed that ion exchange or adsorption/desorption reactions may be responsible for such strong buffering effects. Indeed, many C-Q studies have postulated that ion exchange reactions are responsible for buffering the solute concentrations of infiltrated rainwater in the vadose zone [e.g., *Clow and Mast*, 2010; *Jin et al*., 2011; *Markewitz et al*., 2011; *Herndon et al*., 2015]. Other processes such as displacing (or flushing) the stored water [e.g., *McDonnnell*, 1990; *Burns et al*., 1998] or dissolving readily soluble phases (i.e., amorphous aluminosilicate, calcite) [*Asano et al*., 2003; *Calmels et al*., 2011] are also attributed to the well-buffered soil runoff chemistry.

This soil water may flow laterally in the saturated zone and then drain to the stream as well as infiltrate into the underlying weathered bedrock zone [*Montgomery et al*., 1997; *Montgomery and Dietrich*, 2002; *Uchida et al*., 2003; *Haria and Shand*, 2004; *Tromp-van Meerveld et al*., 2007; *Salve et al*., 2012]. The flow through deeply weathered bedrock zone may be responsible for a significant fraction of stream runoff and chemical weathering flux [*Neal et al*., 1997a; *Anderson and Dietrich*, 2001; *Uchida et al*., 2003; *Tromp-van Meerveld et al*., 2007; *Calmels et al*., 2011], implying its key role in the C-Q relationships as well. In the saturated weathered bedrock zone, water may flow via fractures and thus travel much faster than in the vadose zone [*Anderson et al*., 1997b]. The bedrock groundwater is recharged by the rainwater that already chemically evolved through the vadose zone, which may slow the reaction kinetics; however, material in this zone is fresher than that in the soil layer, thus such effects would be compensated, resulting in further water chemistry evolution in the bedrock zone [*Anderson and Dietrich*, 2001]. *Anderson et al*. [1997a] proposed that groundwater chemistry may be a function of reaction time (linked to transit time) through the bedrock zone. In their study, the groundwater either emerged to the shallow soil layer in the downslope area or directly drained to the stream, mixing with relatively dilute soil water. At the Coos Bay site, the next effect of rapid solute evolution in the vadose zone and modest increase in solutes in the perched groundwater was a nearly flat C-Q relationship at the emerging springs [*Anderson et al*., 1997a]. This study did not, however, look farther downstream to document the C-Q response at the larger watershed level.

All these interpretations about the bedrock groundwater, however, are inferred from indirect observations: groundwater samples were collected at weirs, springs, seeps, or wells near the stream, often at a low frequency [*Anderson et al*., 1997a; *Neal et al*., 1997b; *Burns et al*., 2001; *Asano et al*., 2003; *Haria and Shand*, 2004; *Shand et al*., 2005; *Calmels et al*., 2011]. These measurements cannot fully document water chemistry evolution inside the critical zone, even though the critical zone structure may strongly influence the interpretation of observations. For instance, *Uchida et al*. [2006] proposed that on otherwise similar hillslopes, the mean residence time of runoff aged vertically on deeply permeable bedrock and laterally on low permeability bedrock. Direct observations of groundwater chemistry deep in the critical zone (which often extends up to 20 m deep) paired up with stream chemistry has rarely been done.

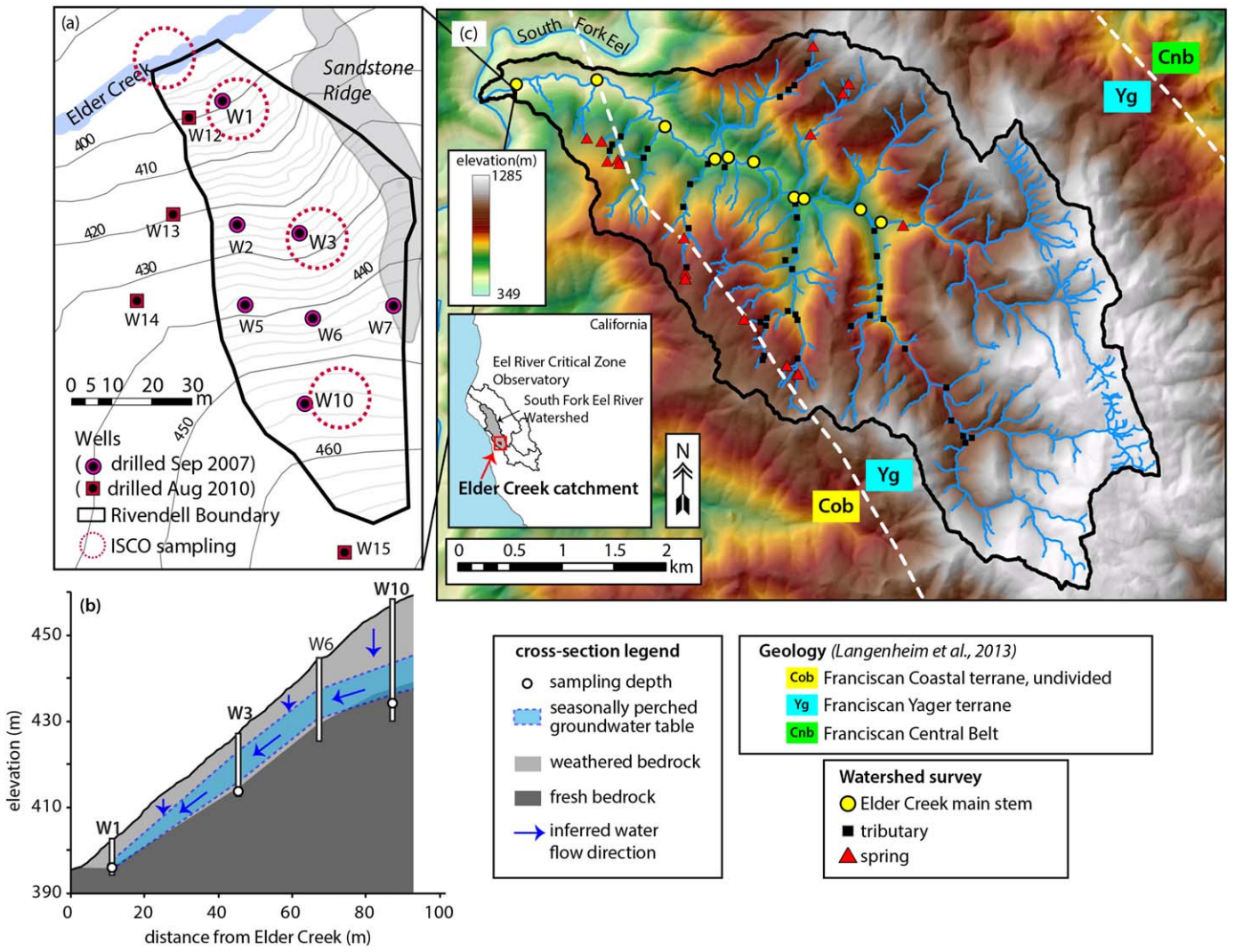

Figure 1. Overview of the study site. Elder Creek (16.8 km^2) is one of the tributaries of South Fork of the Eel River, one of the headwaters of the Eel River Critical Zone observatory in California. (a) Rivendell is a small (4000 m^2) and steep hillslope (average slope 32°) in Elder Creek. A total 12 wells (well 16 not shown) were drilled to fresh bedrock. Water samples of three wells (W1, W3, and W10) along the axis of hillslope and Elder Creek were collected from late 2008 to 2014 at 1–3 days intervals using automated water samplers. (b) Cross section of Rivendell. A seasonally perched groundwater table is developed on the fresh bedrock boundary. Groundwater samples were collected at a fixed location in the permanently saturated zone at each well. The temporal and spatial variability of groundwater chemistry is reported in *Kim et al.* [2014]. (c) The Elder Creek catchment is mainly underlain by Yager terrane and the border between Yager and Coastal terranes crosses the southwest corner of the catchment. Along the stream channel network, water samples—spring (red triangle), tributaries (black square), and Elder Creek main stem (yellow circle)—were collected in May and August 2014.

To address these observational gaps, this study presents parallel observations of stream and bedrock groundwater chemistry monitored at 1–3 day intervals over 4 years (2009–2013) in the Elder Creek catchment in the Eel River Critical Zone Observatory in California (Figure 1). A previous study carried out at Elder Creek [*Kim et al.*, 2014] reported the spatial and temporal variability of groundwater chemistry along a steep hillslope, dubbed Rivendell (Figure 1a), and identified the governing processes for its chemistry. The groundwater chemistry showed strong water table depth dependence (Figure 2): once the groundwater table rose above a certain depth at each well, the solute concentration was diluted up to a factor 10 and remained at these levels until the water table depth receded below this depth. The authors identified two controlling processes for the water chemistry of the groundwater and concluded that their dominance shifts seasonally. At high flow, the cation exchange reactions enhanced by high subsurface pCO_2 and dissolution of amorphous Si rapidly increase the solute concentrations of the infiltrated rainwater in the vadose zone, and this water recharges the groundwater. At low flow, when the groundwater table is low, groundwater may reach equilibrium between primary and secondary minerals and be saturated with calcite under the high pCO_2, thus displaying higher solute (i.e., Ca and Mg) concentrations. In this study, we will compare

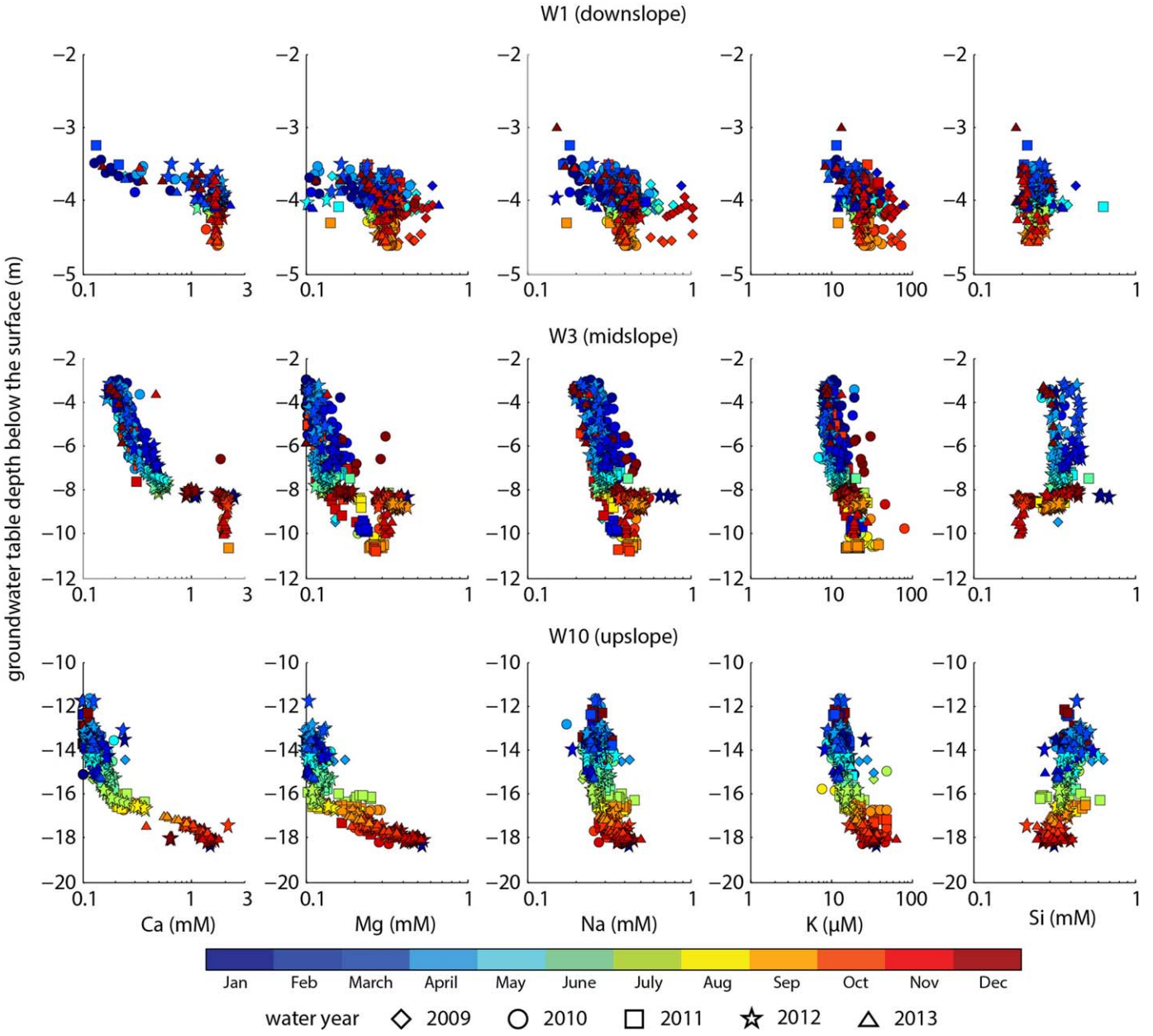

Figure 2. Solute concentrations-depth relationships of groundwater in Rivendell. This data were reported in *Kim et al*. [2014] and here we rotated the reported figure to show the concentration variation (*x* axis) with depth (*y* axis) in a vertical direction with permission. The solute (Ca, Mg, Na, K, and Si) concentrations of W1, W3, and W10 were plotted against the groundwater table depth at the time of sample collection. The markers represent the water year of sample collection and are color-coded by month.

the groundwater and stream water chemistry observations and investigate the role of water chemistry evolution along the critical zone in expressing the C-Q relationships of the Elder Creek catchment.

2. Methods

2.1. Study Site

Elder Creek (16.8 km^2) is a tributary of the South Fork Eel River in the Eel River Critical Zone Observatory in California (Figure 1c). The Elder Creek discharge is monitored at a U.S. Geological Survey (USGS) gauging station, which is located approximately 300 m upstream from the outlet of the catchment. Elder Creek was part of the U.S. Geological Survey's Hydrologic Benchmark Network (USGS-HBN), and its water chemistry was monitored from 1968 to 1996 (Station #11475560) [*Mast and Clow*, 2000]. Elder Creek is part of the

Angelo Coast Range Reserve, which is managed by the University of California Natural Reserve System (UCNRS). The reserve is mostly forested with a few patches of meadows: Douglas fir (*Pseudotsuga menziesii*), tanoak (*Lithocarpus densiflorus*), live oak (*Quercus* spp.), California bay (*Umbellularia californica*), and madrone (*Arbutus menziesii*) cover most of the upper slopes; redwoods are found near the stream channel (*Sequoia sempervirens*); and native and European grasses cover the meadows (Natural History in Angelo Coast Range Reserve, UCNRS; http://angelo.berkeley.edu). The climate is a typical Mediterranean regime—a warm and dry summer contrasting with a cool and wet winter. The mean annual precipitation for the study period (2009–2013), measured at the meadow across from the study location, was 1760 mm yr^{-1}, and the long-term average is approximately 1900 mm yr^{-1}[*Salve et al*., 2012].

Most of Elder Creek is underlain by Yager terrane of the Coastal Belt of the Franciscan formation, an Eocene age assemblage of marine argillite, graywacke, and conglomerate (Figure 1c) [*Mclaughlin et al*., 2000; *Langenheim et al*., 2013]. The graywacke is arkosic to lithic. Based on extensive walking of the channel network in Elder Creek, *Lovill* [2016] found that the sandstone and conglomerate make up less than 30–40% of the watershed, the rest being underlain in argillite. The boundary between the Yager and the more western Coastal terrane of the Coastal Belt crosses just upstream of the mouth of Elder Creek (Figure 1c). Our intensive monitoring site (Rivendell) is located on that Coastal terrane, just to the west of the Yager. Rivendell is primarily underlain by argillite but is bordered by a ridge of sandstone (Figure 1a). The composition of the Yager and Coastal terranes is considered to be very similar. *Underwood and Bachman* [1986] proposed that the two terranes share the same provenances and that sediments of the Yager were deposited associated with submarine channels that crossed the Coastal terrane (see *Mclaughlin et al*. [2000] for further description). The Coastal terrane is distinguished by being more internally deformed than the Yager and has more laumontite veins.

Detailed descriptions of Rivendell, where groundwater hydrochemistry was intensively monitored, can be found in *Salve et al*. [2012] and *Kim et al*. [2014]. Rivendell is a small and steep hillslope (4000 m^2; average slope 32°), with a thin soil layer (0.5–0.75 m) underlain by thick, weathered argillite (5–25 m; Figure 1b). All runoff is generated through the weathered argillite zone via fractures [*Salve et al*., 2012]. Twelve wells were drilled into fresh bedrock (Figure 1a) and were cased with perforated polyvinyl chloride (PVC) pipes (detailed well installation can be found in *Salve et al*. [2012]). Since the well installation in 2008, soil moisture, soil temperature, climate variables, tree-sap flow, groundwater level, and groundwater temperature have been continuously monitored at high frequency (5–30 min; http://www.sensor.berkeley.edu).

2.2. Collection of Stream and Groundwater Samples at Rivendell

Detailed water sampling protocols, sample handing, and sensor calibration can be found in *Kim et al*. [2014]; here, we briefly summarize the protocol. From October 2008 to January 2014, water samples of W1, W3, W10 (each well is labeled with the letter "W" and a number; Figure 1a), and Elder Creek were collected using automated samplers (ISCO 6712 sampler; Teledyne ISCO, Lincoln, NE) with a modified custom remote operating controller [*Kim et al*., 2012]. Elder Creek and W1 were sampled simultaneously. The sampling frequency was 1–2 days during the wet season and 2–3 days during the dry season. Occasional larger sampling gaps occurred, especially in the last year of monitoring, due to power, sampler, or submersible pump failures (Figure 3). Bulk rainwater and throughfall were collected at an open meadow across from Rivendell and under the forest at the W7 area, respectively. On every ISCO deployment date, reference samples were collected, following a standard water sampling method for trace metals (i.e., immediate filtration and acidification) [*U.S. Environmental Protection Agency*, 1996]. The temperature and pH of the reference samples were also measured using a portable pH meter (Fisher Scientific Accumet™ AP115 Portable pH).

At the beginning of the project, $CaCO_3$ precipitation in ISCO samples, collected using ISCO ProPak® LDPE 1000 mL bags, occurred at W1 and W3. After October 2011, a new sampling method was used—a gravitational filtration system (GFS) that filters samples (Supor PES membrane disc filter, 0.45 μm pore size, Pall Corporation) by gravity upon sampling. This method maintains the sample integrity not only for Ca but also for trace metals [*Kim et al*., 2012]. In this study, we report all the Elder Creek data (major cations and Si) because the integrity of these elements in the creek samples was well maintained independent of the sampling method.

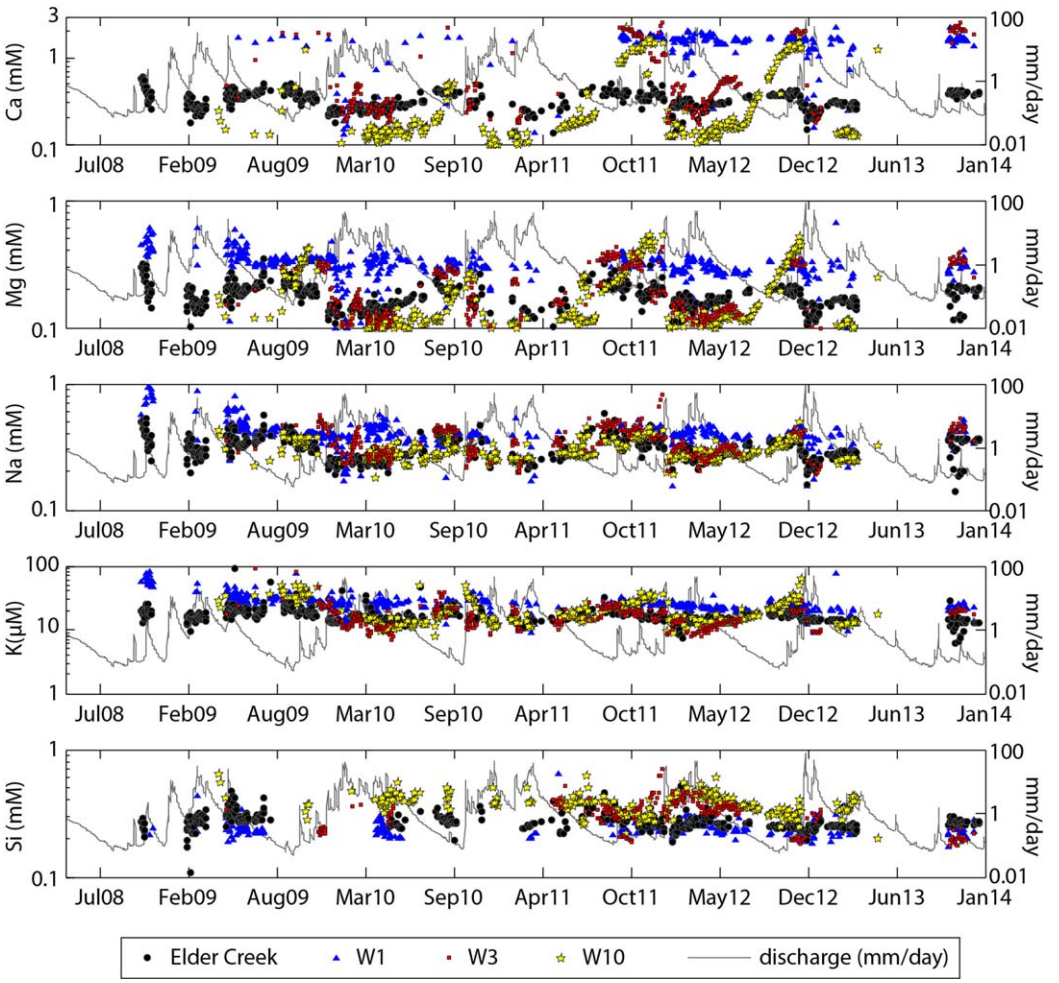

Figure 3. Time series of major cations and Si of Elder Creek (closed circle), W1 (blue triangle), W3 (red square), and W10 (yellow star). The Elder Creek discharge is shown in a gray line.

2.3. Watershed Surveys

We investigated the water chemistry of springs, tributaries, and the main stem of the Elder Creek catchment from 25–29 May (68 total locations) to 18–23 August (55 total locations) in 2014 (Figure 1c). These surveys were designed to compare the solute concentrations of the local springs, tributaries, and upstream of the main stem of Elder Creek to those of Rivendell. At each survey location, the temperature and pH of water samples were measured using the portable pH meter. The water samples were filtered upon collection using an all-plastic 12 mL syringe and the same filters as the ISCO sampling. The samples were taken at locations that were either as close as possible to the center of the channel or at an alternate location where the least amount of sediment would be collected. The drainage area to each sample location was estimated from the surface area that drains to the sample point. Spring surface drainage area may differ from the actual contributing drainage area.

2.4. Water Chemistry Analysis

All the water samples were analyzed for major cations and minor and trace elements using a Finnigan Element II magnetic sector inductively coupled plasma-mass spectrometer (ICP-MS) in Lawrence Berkeley National Laboratory. All the samples were acidified (2% v/v nitric acid). Indium (In; 1 ppb) was used as an internal standard. To evaluate the accuracy and precision of the analysis, Certified River Water Reference Material for Trace Metals, SLRS-5 (National Research Council (NRC), Ottawa, ON, Canada), was included in every sample analysis. The achieved % accuracy of this study was 99 ± 10% (Ca), 100 ± 10% (Mg), 97 ± 14% (Na), 96 ± 13% (K), and 105 ± 7% (Si).

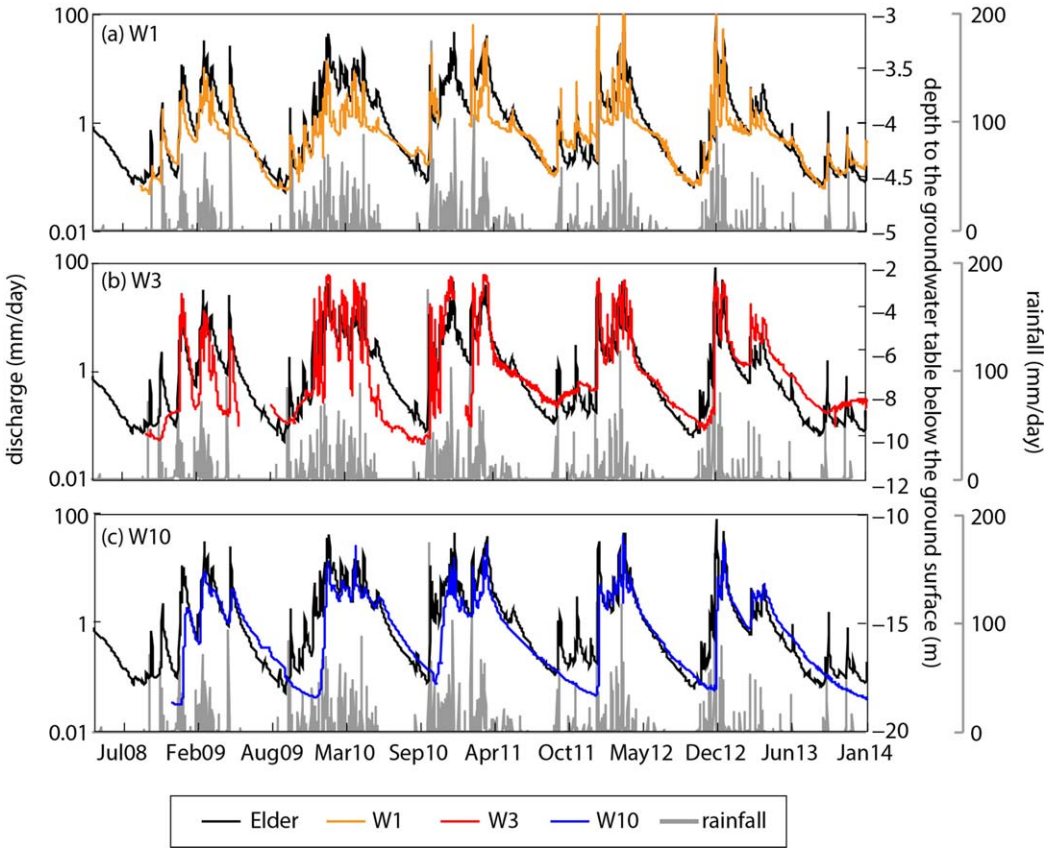

Figure 4. Hydrometric observations at (a) W1, (b) W3, and (c) W10. Precipitation (gray bar) and Elder Creek (black solid line) discharge are shown in each plot as well for comparison.

3. Background: Summary of Rivendell Groundwater Hydrochemistry

The Rivendell groundwater hydrochemistry was discussed extensively in *Kim et al*. [2014] and here we briefly summarized the groundwater observations for the comparison with those of Elder Creek. During the wet season, when more than 95% of rainfall is delivered, Elder Creek was highly responsive to rainfall inputs: discharge increased by four orders of magnitude (from 0.01 to 100 mm d^{-1}; Figures 3–5). The W1 groundwater table fluctuated by 1–1.5 m synchronously with Elder Creek's discharge (Figure 4a). In contrast, W3 and W10 required 2–3 months of lag time after the first major rainstorm of the season to significantly raise their water tables (by 4–6 m; Figures 4b and 4c). This lag was due to early rains mostly contributing to increasing soil and rock moisture [*Salve et al*., 2012; *Rempe*, 2016]. After an initial rise in response to winter rains, the W3 and W10 water tables fluctuated within −3 to −7 m and −12 to −14 m below the ground surface.

As noted *Kim et al*. [2014], W1 (closest to the channel) is systematically different from W3 and W10, and here we see that W1 also typically has much higher cation concentrations than Elder Creek (Figure 3). Furthermore, W1 water chemistry was invariant year round except for a few dilution events. *Kim et al*. [2014] showed that the difference between W3 and W1 could not be due to chemistry evolution from W3 to W1 but instead proposed that W1 likely records fluids strongly influenced by the adjacent sandstone ridge (Figure 1a). The soil mantle at W1 is rich with fractured sandstone colluvium. The data presented here also further support that inference by showing that in contrast to W1, the solute concentrations of W3 is much more similar to those of Elder Creek.

Rainwater introduces insignificant amount of solutes: the volume-weighted concentrations average 0.003 mM (Ca), 0.005 mM (Mg), 0.032 mM (Na), 5 μM (K), and 0.003 mM (Si) [*Kim et al*., 2014, Table 2]. As this rain passes through tree canopy, the concentrations of Mg, Na, and Si increased by less than a factor of two while Ca was enriched by a factor of three. The K concentration in throughfall, however, was higher than that of bulk rain by factor of six. The throughfall K values exceeded the winter and summer groundwater

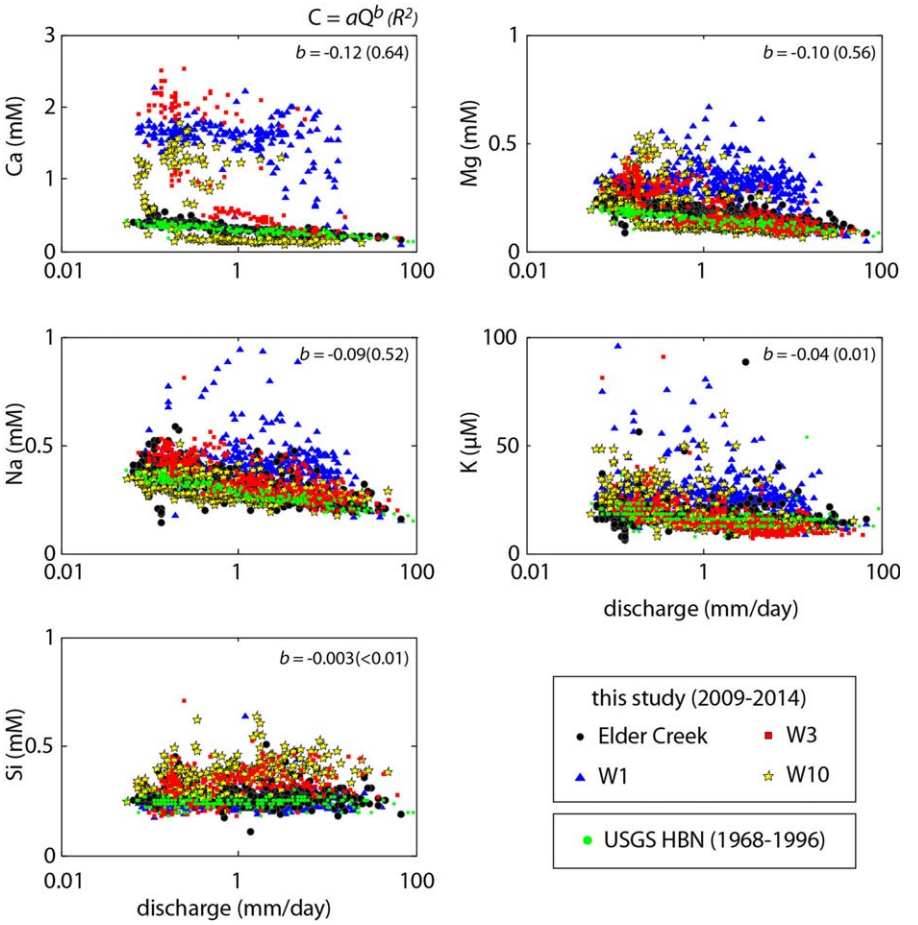

Figure 5. Concentration-discharge (C-Q) relationships of Elder Creek (black circle). The C-Q of the USGS HBN Branscomb data (green circle), W1 (blue triangle), W3 (red square), and W10 (yellow star) are shown for comparison here. The exponents (*b*) and R^2 of power law fits to the C-Q for our measurements in Elder Creek are shown in each plot. Groundwater concentrations are plotted against Elder Creek discharge at the time of sample collection is used. Figures of individual C-Q relationships can be found in supporting information figures.

concentrations likely due to leaching from tree canopy. Significant enrichment of K in throughfall has been well documented [*Likens et al.*, 1994; *Tobon et al.*, 2004; *Macinnis-Ng et al.*, 2012]. Potassium is an essential nutrient and can easily leached out from leaves because it plays a role as an electrolyte in trees [*Likens et al.*, 1994]. Solute concentrations of groundwater (i.e., W3 and W10) varied seasonally as their water tables rise and fall (Figure 2). During the high winter groundwater (i.e., W3 and W10), the solute concentrations of groundwater are higher than those of throughfall by factor of 5–24 (except for K) and these values are lower than the maximum values at the lowest groundwater table level by factor of 8–11 (Ca), 3–4 (Mg), 1.3–1.9 (Na), 2.3 (K), and 0.7–0.8 (Si) [*Kim et al.*, 2014].

4. Results

4.1. The C-Q Relationship of Elder Creek

The concentrations of major cations and Si of Elder Creek showed typical chemostatic features (Figure 5; see supporting information Figures S1–S4 for data plotted separately for each well). Elder Creek's Ca, Mg, Na, and K concentrations slightly decreased with increasing discharge (typically less than a factor of two over the entire discharge range) while the discharge fluctuated by four orders of magnitude. The USGS-HBN C-Q relationships are similar to ours (Figure 5). The concentration variation with discharge was fitted with a power law regression ($C = aQ^b$) [*Godsey et al.*, 2009]. The exponents for this study's observations and USGS-HBN data different insignificantly (95% confidence interval): the exponents (*b*) of our observations versus USGS-HBN measurements are −0.12 versus −0.12 (Ca), −0.10 versus −0.11 (Mg), −0.09 versus

Table 1. Summary of Exponents of Power Law Function Fittings of Concentration-Discharge Relationships of Elder Creek

	Exponents[a] (95% Confidence Interval)				
Data Source	Ca	Mg	Na	K	Si
This study	−0.12 (−0.13, −0.11)	−0.10 (−0.11, −0.09)	−0.09 (−0.10, −0.09)	−0.04 (−0.05, −0.03)	0.00** (−0.01, 0)
USGS HBN[b]	−0.12 (−0.13, −0.11)	−0.11 (−0.12, −0.10)	−0.11 (−0.12, −0.10)	−0.05 (−0.06, −0.03)	0.00** (−0.01, 0.01)

[a]Exponents of power law fittings of concentration-discharge relationships. All the exponents were statistically significant (near zero *p*-values) except for **Si of Elder Creek.
[b]USGS HBN Branscomb measurements.

−0.11 (Na), and −0.04 versus −0.05 (K; Table 1). These values were statistically significant (*p*-values <0.005). The R^2 varied from 0.64 (Ca), 0.56 (Mg), 0.52 (Na), and 0.01 (K), respectively. Si in Elder Creek showed nearly ideal chemostatic characteristics ($b = -0.003$ (this study) versus 0.0001(USGS-HBN)) (Table 1) and the exponents for both data sets were insignificantly different from 0.

4.2. Watershed Survey of the Solute Chemistry of Springs, Tributaries, and the Main Stem

The May and August surveys revealed that as the cumulative drainage area increased, the solute concentration converged to the Elder Creek concentrations at the downstream main stem also where time series samples were collected (Figure 6). For instance, the solute concentrations of the main stem for the May survey averaged 0.35 mM (Ca), 0.18 mM (Mg), 0.31 mM (Na), 16.9 μM (K), and 0.25 mM (Si) and their coefficients of variation (CV) were 3–4% (Table 2). This convergence indicates that the main stem of Elder Creek is well mixed. In contrast, the spring water, which comes from local groundwater, displayed variable solute concentrations (Figure 6). The solute concentrations of the springs for the May survey, for instance, averaged 0.27 mM (Ca), 0.16 mM (Mg), 0.31 mM (Ca), 15.6 μM (K), and 0.34 mM (Si) and their CVs varied between 19% and 53% (Table 2). The solute concentrations of the August survey were slightly higher than those of the May survey perhaps due to declining base flow and deeper groundwater being released. The spring water tended to be somewhat lower in K and higher in Si concentrations than the mainstream Elder Creek (Table 2).

The spring and tributary concentrations varied within the ranges that we observed in the Rivendell groundwater. Figure 7 shows histograms of the solute concentrations of Rivendell groundwater and all the springs for the same discharge (0.4–0.5 mm d^{-1} for the May survey and 0.05–0.1 mm d^{-1} for the August survey) for all 4 years, but not the same day. The high correlation between discharge and concentration enables us to use all our groundwater measurements close to these two discharges (for the entire monitoring period) and thus create a concentration distribution function to compare with the watershed survey. For comparison in Figure 7, the spring's distributions were showed as green shaded areas and those of Rivendell groundwater were displayed as lines. Calcium (Ca) showed the largest differences between Rivendell groundwater and the springs. The highest Ca concentration of spring water was 0.71 mM while Ca in the Rivendell groundwater for the August survey discharge was much greater than 1 mM (1.7–2.5 mM). Such a difference might actually reflect spatial heterogeneity; however, we propose below, based on our sampling experience at Rivendell, that Ca in the spring water was lower because of calcite precipitation due to CO_2 degassing. The high K concentrations in W3 groundwater may be due to K leaching from the tree canopy caused by the first rainstorm that occurred in September and October. Other than Ca and K, the concentrations of Mg, Na, and Si of the springs varied within the range of those of Rivendell groundwater (Figure 7). Collectively, we conclude that even though Rivendell covers only 0.02% of the catchment, its water chemistry can represent the groundwater chemistry for the whole catchment.

4.3. Groundwater Versus Stream Chemistry Dynamics

In order to compare the concentrations in the groundwater with those in Elder Creek, we used the Elder Creek discharge specifically at the time of the groundwater sampling (Figure 5). As mentioned previously, there is considerable delay in response to storm events at the upslope wells compared to Elder Creek [*Rempe*, 2016]. In addition, the travel time from W3 and W10 to Elder Creek may be months, especially at low flow. Hence, the correlation suggested in Figure 5 could be problematic. The maximum variation of concentration in the wells, however, is small compared to the discharge range, and the conclusion that the groundwater is also close to chemostatic (except for Ca) is not affected by this timing uncertainty.

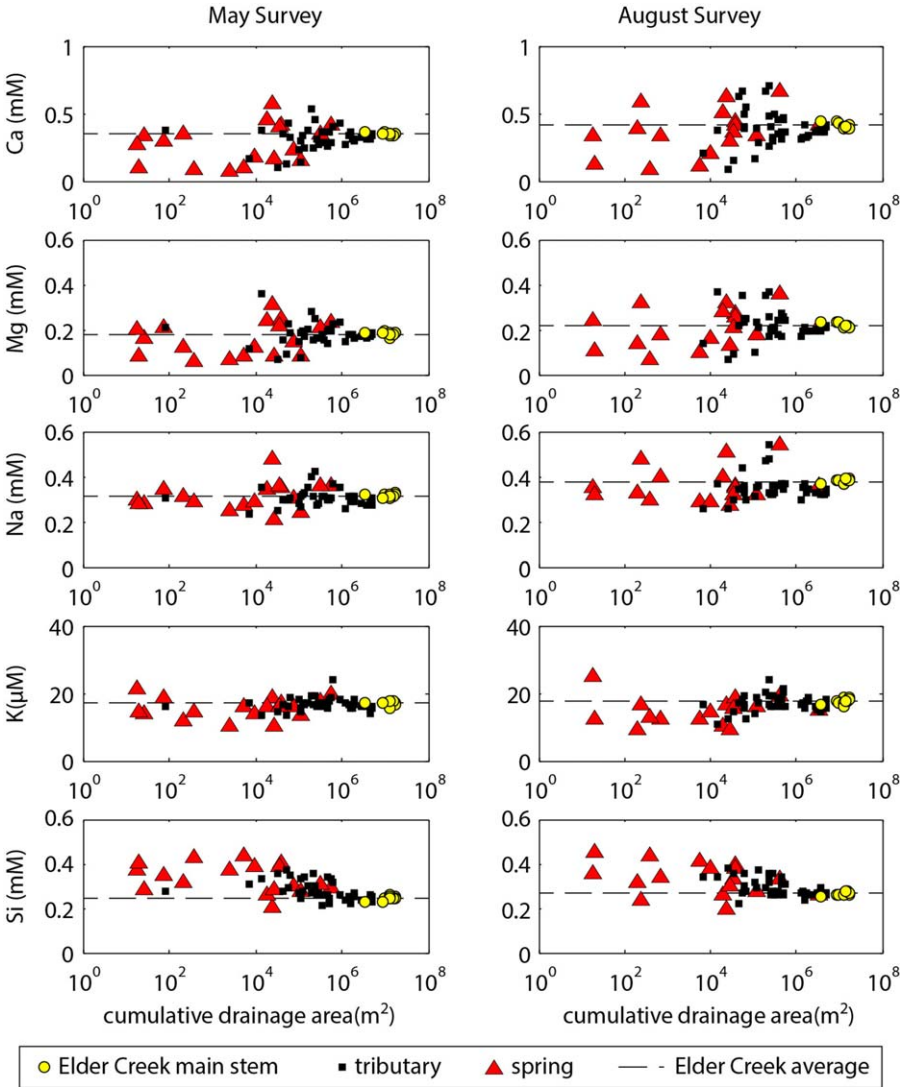

Figure 6. Solute concentrations of springs (red triangle), tributaries (closed square), and Elder Creek main stem (yellow circle) as a function of cumulative drainage area.

We push this comparison even more quantitatively by plotting the ratios of the cation concentrations in a specific well compared to those of samples from Elder Creek that were typically collected within hours (Figure 8). The averages of these ratios at a 0.5 m interval are also shown in supporting information Figures S5 and S6. The ratio value of 1:1 is shown as a solid vertical line. Note that in Figure 8, each point is color-coded by the Elder Creek discharge at the time of sampling so that it is possible to detect differences

Table 2. Averages and Coefficients of Variation of Solute Concentrations of Springs, Tributaries, and Main Stem of Elder Creek

	Ca (mM)		Mg (mM)		Na (mM)		K (μM)		Si (mM)	
	May	Aug	May	Aug	May	Aug	May	Aug	May	Aug
Average										
Springs	0.27	0.42	0.16	0.24	0.31	0.39	15.6	15.3	0.34	0.32
Tributaries	0.31	0.39	0.18	0.22	0.31	0.35	16.7	16.8	0.28	0.30
Main stem	0.35	0.41	0.18	0.22	0.31	0.38	16.9	17.5	0.25	0.27
Coefficient of variation (%)										
Springs	53	35	47	33	19	21	20	24	19	19
Tributaries	27	39	28	33	12	16	11	16	15	16
Main stem	3	5	4	4	3	2	4	4	4	4

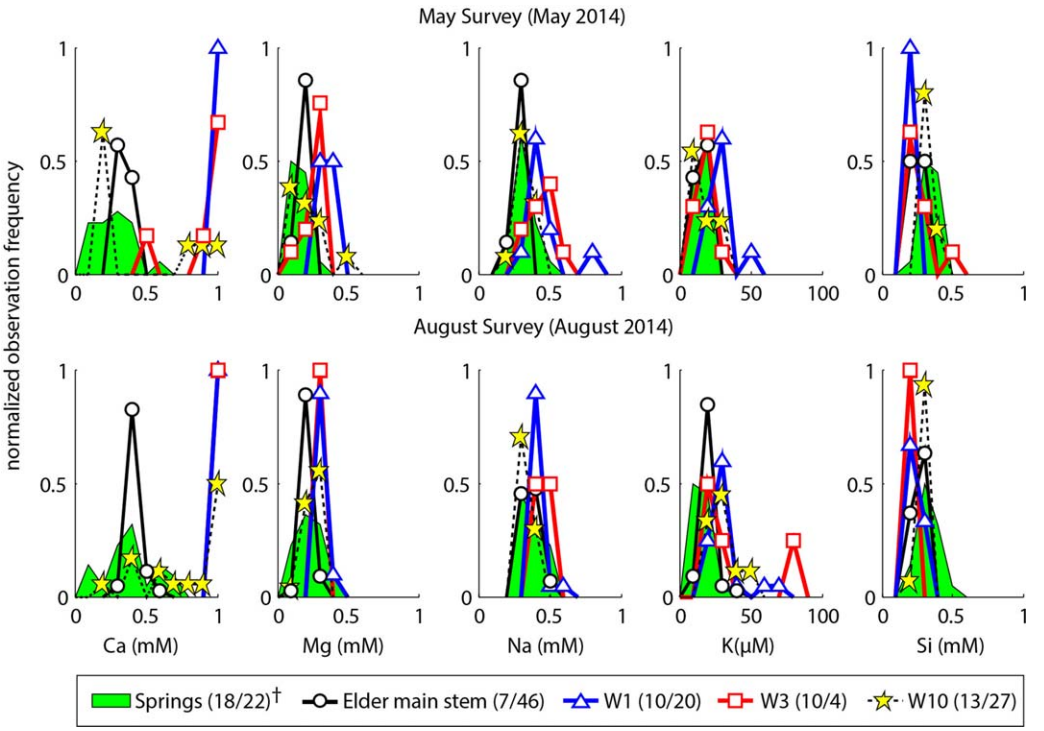

Figure 7. Concentration distributions of major cations and Si of springs (green shaded area) in the Elder Creek catchment. For comparison, the concentration distributions of W1 (blue triangle), W3 (red square), W10 (yellow star), and Elder Creek (open circle) at the Elder Creek discharge of each heterogeneity are shown as well. †The numbers of observations of the histograms are shown in the parentheses (May/August survey).

between high and low flow. This color-coding reveals a similar structure to that reported in Figure 2. The highest groundwater level corresponds to the highest flows. There are exceptions in W3 and W10 that arise early in the wet season when Elder Creek discharge increases but the upslope groundwater systems have not yet responded.

During low flow, when the groundwater table declined below −8 m (W3) and −16 m (W10), the concentrations of Ca, Mg, and K in groundwater were higher than those of Elder Creek. For example, W3 displayed higher solute concentrations than those of Elder Creek by, on average, factors of 4.62 (Ca), 1.46 (Mg), and 1.47 (K; Table 3). The large difference in Ca can be attributed to calcite precipitation of the groundwater as it emerges at the streamside. For example, in August 2011, when the W3 water table was about −8 m, samples taken using the W3 GFS prototype, a new method that is capable of preserving sample integrity for Ca, had 2–2.5 mM of Ca, which is the saturation level under the W3 headspace pCO_2 (4–6%) and its pH (6.8; open system; Figure 9). In contrast, the ISCO ProPak bag samples—a conventional sampling method in which CO_2 was degassed and Ca was precipitated—showed 0.85–1.4 mM of Ca. The subsurface pCO_2 in Rivendell was approximately two orders of magnitude higher than that of the atmospheric level [*Kim et al*., 2014], likely due to biological activities (e.g., organic matter decomposition by microbial metabolism and tree respiration). Therefore, groundwater loses Ca as it emerges to the surface because of CO_2 degassing, resulting in such large differences in Ca concentrations between the groundwater and Elder Creek.

At high winter runoff, these elements in groundwater and the stream are similar to or slightly lower than the Elder Creek concentrations. For example, W10 had lower concentrations compared to those of Elder Creek by factors of 0.5 (Ca), 0.68 (Mg), 1.01 (Na), and 0.94 (K) while W3 showed similar solute concentrations to those of Elder Creek (Table 3). The lower values at high flow in W10 than those in W3 (which are more like the stream flow) maybe due to the evolution of water chemistry en route to Elder Creek. Although groundwater head analysis suggests that W10 does not flow toward W3 [*Rempe*, 2016], W3 is approximately 50 m from the nearest channel bank while W10 is about 90 m. This considerable difference in travel distance may contribute to the lower ratios of W10 than those of W3 if lateral evolution of the groundwater occurs. Additionally, some mineralogical differences between Rivendell weathering bedrock and the weighted average of the entire catchment may exist and influence solute release as a function of discharge.

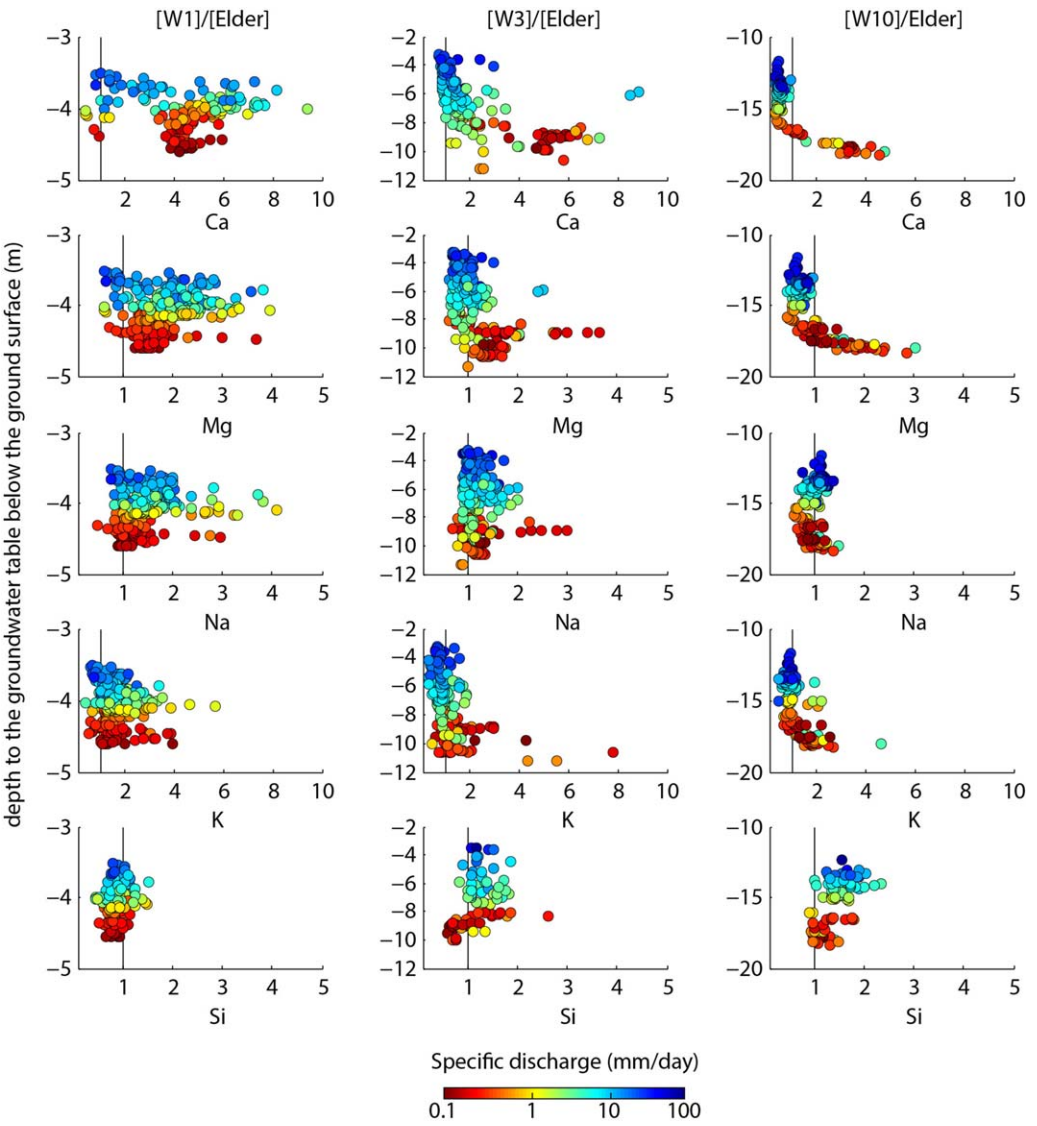

Figure 8. Ca, Mg, Na, K, and Si concentration ratios of Rivendell groundwater to Elder Creek. The groundwater depth (*y* axis) indicates the groundwater table at the time of groundwater sample collection. The paired groundwater and stream samples were collected within hours at the same day. The color represents Elder Creek's specific discharge at the time of sampling.

5. Discussion

5.1. Controlling Processes for Chemostatic Behavior in Elder Creek

The power law exponents of the C-Q relationships for all major cations and Si were between −0.12 and −0.003, demonstrating the relatively invariant solute chemistry with a large range of discharge in Elder

Table 3. Average Ratios of Solute Concentrations Between Groundwater and Elder Creek at High and Low Flows

Flow Regime	Groundwater Depth (m)	Ca	Mg	Na	K	Si
[W3]/[Elder]						
High flow	>−8	1.46 (1.06)[a]	0.94 (0.27)	1.20 (0.24)	0.84 (0.30)	1.32 (0.24)
Low flow	<−8	4.62 (1.51)	1.46 (0.54)	1.27 (0.41)	1.47 (1.02)	1.03 (0.49)
[W10]/[Elder]						
High flow	>−16	0.50 (0.10)	0.68 (0.11)	1.01 (0.16)	0.94 (0.26)	1.57 (0.26)
Low flow	<−16	2.65 (1.24)	1.45 (0.56)	1.01 (0.17)	1.60 (0.59)	1.23 (0.28)

[a]Standard deviations are shown in parentheses.

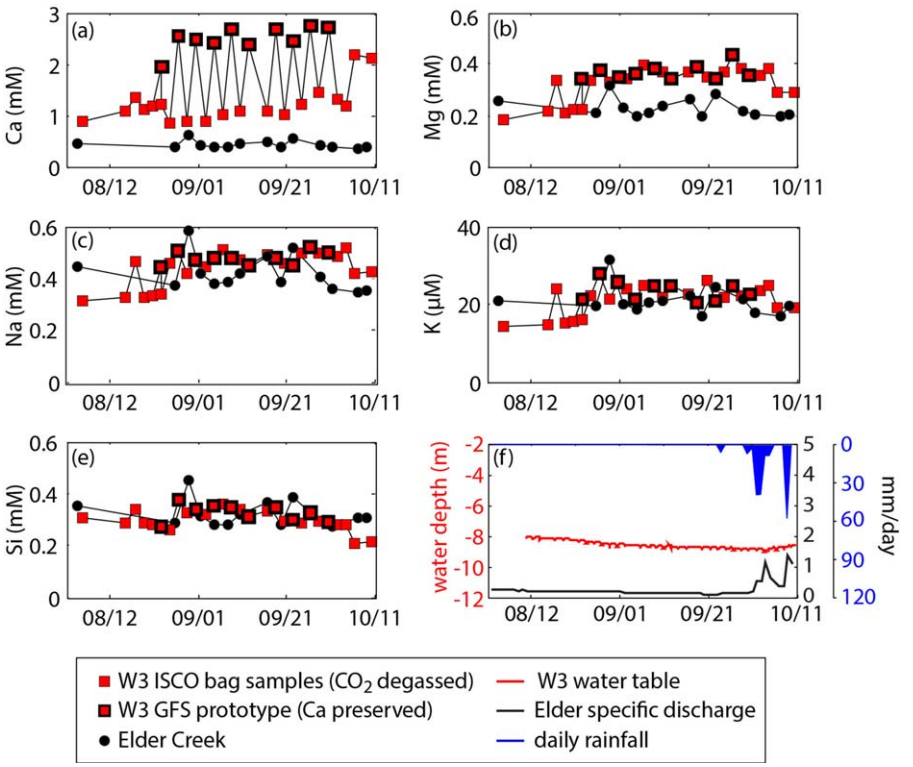

Figure 9. Concentrations of (a) Ca, (b) Mg, (c) Na, (d) K, and (e) Si in W3 collected using the ISCO bag samples (red square; CO_2 degassed) and the GFS prototypes (red square with black box; precipitated $CaCO_3$ recovered) in August–September 2012. For comparison, the solute concentrations of Elder Creek for the same period are shown in closed circles. (f) Elder Creek discharge (black), W3 water table (red), and rain events (blue) during the present sampling period.

Creek (Figure 5). *Kim et al*. [2014] identified two controlling processes for the groundwater chemistry in the Elder Creek catchment. These two processes operate in two respective locations in the critical zone structure. In this study, the comparison between groundwater and stream water chemistry demonstrates that these two processes may also dictate the highest and lowest limits of solute concentrations of the stream, thus resulting in chemostatic characteristics.

At the beginning of the wet season, during the lowest flows in Elder Creek, the concentrations of cations in the groundwater and stream are highest (Figure 10a). The groundwater slowly drains in the deepest saturated zone, due to reduction in the fracture density and aperture with increasing depth [*Salve et al*., 2012]. The solute concentrations are similar in successive years at low flow, and there is a tendency in several elements in the groundwater to reach a constant value with continued slow groundwater drainage, suggesting an approach to quasiequilibrium with the mineral assemblages (as described by *Kim et al*. [2014]). The Ca concentration is much higher in the groundwater than in the stream due to calcite precipitation and CO_2 degassing as the groundwater emerges at springs.

During the wet season, the first rains mostly go into storage in the thick (4–18 m deep) vadose zone, evidenced by the delayed groundwater rise (Figure 4) [*Kim et al*., 2014], stable isotopic mixing [*Oshun et al*., 2016], and direct measurement by neutron probe surveys [*Rempe*, 2016]. Arriving rainwater into the vadose zone experiences elevated pCO_2 which drives high H_2CO_3 and cation exchange reactions (as shown by application of PHREEQC analysis by *Kim et al*. [2014]; Figure10b). This occurs as the groundwater in the upslope region continues to recede despite the onset of the rainy season. Once the vadose zone storage reaches a characteristic amount ($\sim$ after 400 mm of cumulative rain; *Kim et al*. [2014]; see *Rempe* [2016] for specifics), subsequent rainwater mixes and displaces water that travels relatively rapidly along fractures and recharges the groundwater [*Salve et al*., 2012; *Rempe*, 2016]. As the groundwater table rises, this newly recharged groundwater becomes the dominant flow in the much more conductive weathered bedrock in the shallower levels of the critical zone (Figure 10c). These waters drain to the stream, apparently without

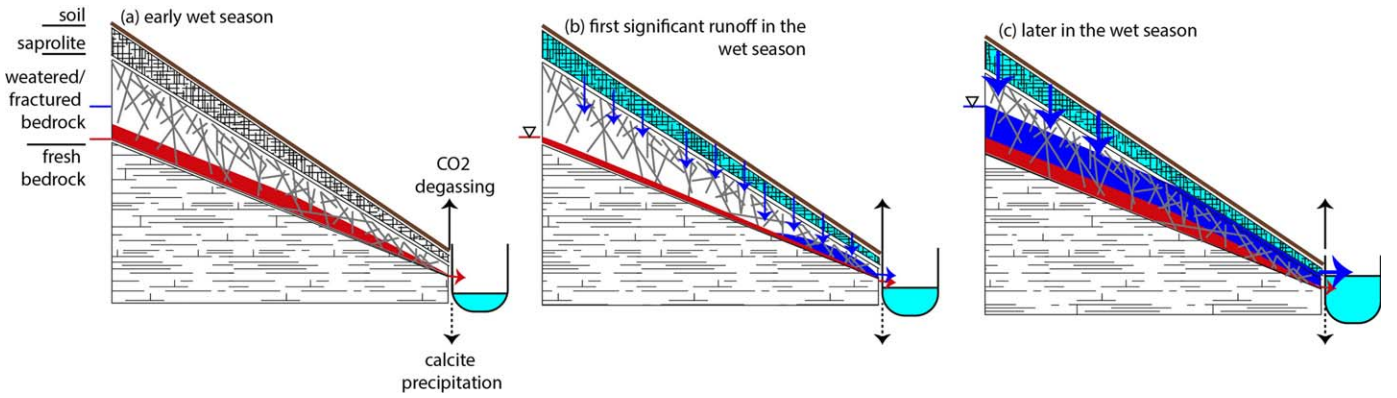

Figure 10. Conceptual model of water chemistry evolution through the critical zone to stream in the Elder Creek catchment. (a) During the early wet season, both groundwater table and Elder Creek discharge are low. Groundwater flows slowly along the fresh bedrock boundary, and has high solute concentrations. This water may even reach equilibrium between primary and secondary minerals and be saturated with calcite under high subsurface pCO_2. When this groundwater emerges to the surface, due to CO_2 degassing, groundwater loses Ca as calcite precipitation. The concentrations of solutes in groundwater are much higher than that in Elder Creek. During this time, any rainwater is mainly stored in the vadose zone. (b) After the vadose zone water storage reaches a critical level, additional rainwater causes relatively rapid recharge to the groundwater and the generation of storm runoff. The chemistry of mobile water may be controlled by interactions with the stored water, likely via ion exchange reactions. (c) Later in the wet season, the groundwater table rises to the highly conductive weathered bedrock zone and water may flow quickly without further chemical evolution. During this time, stream and groundwater have similar chemistry.

further significant chemical evolution, as evidenced by the insignificant concentration differences among the stream, W3, and W10 at high flow (Figure 8). These high runoff flows cause a modest decline of stream concentration yet a large increase in runoff. Because of the rapid cation exchange reaction in the vadose zone, the maximum decline in concentration is, on average, about a factor of 2. Hence, the chemostatic behavior in Elder Creek results from the narrow range of concentrations bounded at one end by relatively rapid cation exchange processes and on the other by the constraints of thermodynamic equilibrium (Figure 11a). Degassing-induced Ca precipitation further limits the concentration range of that element.

The chemostatic behavior of Si in Elder Creek is driven by the same geochemical dynamics, but the near ideal chemostatic behavior may also be influenced by secondary mineral precipitation. *Kim et al.* [2014] showed that the Si concentration in groundwater was high at high flow and low at low flow, which was the opposite pattern of those of cations (Figure 2). They proposed that secondary mineral precipitation, likely that of metastable aluminosilicate, may decrease the Si concentration as the residence time of groundwater increases. The higher Si concentrations in groundwater compared to that of Elder Creek during high flow (Figure 8), when the fast-flowing groundwater dominates the contribution to the stream runoff, suggest that the secondary mineral precipitation may also occur in the stream as well. The spatial distribution of Si concentration across the watershed also supports this hypothesis. Unlike other major cations, the Si

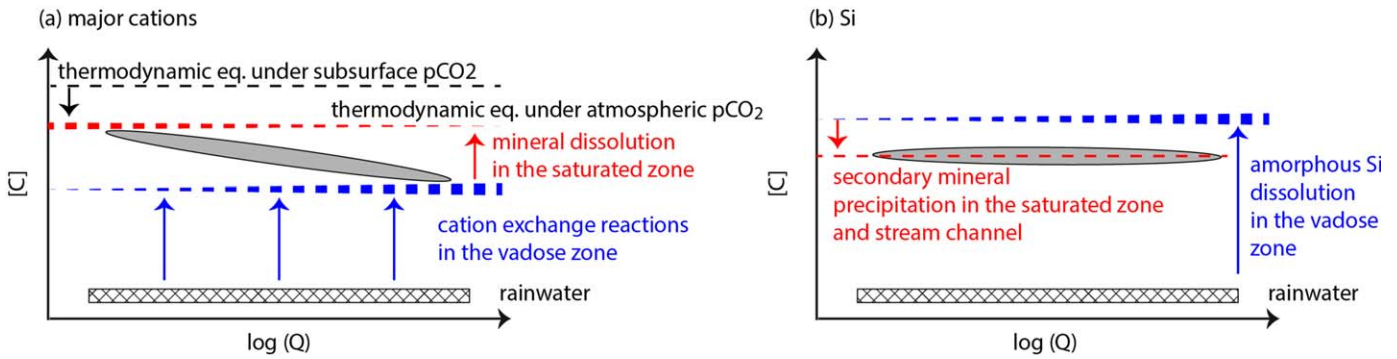

Figure 11. Controlling processes for the chemostatic behavior of major cations and Si in the Elder Creek catchment. (a) The infiltrated rainwater acquires major cations rapidly via cation exchange reactions (exchanged by protons provided by pCO_2) in the vadose zone (horizontal dashed blue line). In the deep fractured bedrock zone, the recharged rainwater concentrates solute further by interacting with less weathered bedrock materials, reaching equilibrium with primary and secondary minerals, and saturation with calcite under high pCO_2. This water sets the upper boundary of the major cation concentrations (horizontal dashed black line). In case of Ca, due to CO_2 degassing, calcite precipitation occurs as the groundwater emerges to the stream, lowering the Ca concentration (horizontal dashed red line). (b) As rainwater passing through the vadose zone, dissolution of amorphous Si phases rapidly increase rainwater's Si concentration (horizontal dashed blue line). Si concentrations of groundwater and stream water are lower than that in the vadose zone due to precipitation of aluminum silicate phases (e.g., metastable aluminum silicate) (horizontal dashed red line).

concentrations of the springs and tributaries, except for 2 cases, were higher than or equal to that of the Elder Creek main stem (Figure 6). This indicates that the decrease of Si as cumulative drainage area increases cannot be explained by mixing with lower Si waters. Altogether, our observations suggest that secondary mineral precipitation may control the near-chemostatic Si concentration in Elder Creek.

Maher [2011] proposed that the balance between time to reach equilibrium and mean transit time of a catchment may dictate the C-Q relationships: if a catchment's mean transit time is sufficiently longer than the equilibrium time, the C-Q will display chemostatic patterns. The author examined this hypothesis for Si only and took Elder Creek as one of the examples of chemostatic catchments. Our observations support the important role of equilibrium between primary and secondary minerals in controlling Si concentrations but may indicate different underlying control for it. We do not have transit time measurements; thus, we cannot directly test Maher's hypothesis. However, our observations imply that Si achieves equilibrium because dissolution of highly reactive Si phases in the vadose zone causes oversaturation with respect to metastable Si phases, resulting in secondary mineral precipitation (Figure 11b). Rapid release of Si in the soil layer has been reported from other study sites as well [e.g., *Kennedy*, 1971; *Asano et al*., 2003].

5.2. Quantification of Chemical Weathering Fluxes

We quantified the chemical weathering fluxes from the vadose zone and the deeper groundwater zone based on the stream and groundwater chemistry observations. Here we define the chemical weathering flux as the sum of solute flux (dissolved phase) and losses of Ca from the deeper groundwater and those of Si from the vadose zone flow. Our observations demonstrated that during the dry season, Ca precipitates from the deeper groundwater as it emerges to the surface. In contrast, Ca in the vadose zone flow behaves conservatively because Ca in this water is too dilute to be oversaturated with respect to calcite even after CO_2 degassing.

Here we took two different approaches to partition the chemical weathering fluxes of the vadose zone and deeper groundwater zone to estimate the minimum and maximum contributions from each zone. In the first approach, we assumed that the Elder Creek discharge is primarily feed by hillslope runoff that behaves similar to W3. We selected W3 as a representative well because its solute concentrations were similar to those of Elder Creek during the wet season (Figure 8 and supporting information Figure S5), indicating that W3 and Elder Creek are well connected. In addition, W3's solute concentrations showed strong depth dependency; thus, the vadose and deeper groundwater flows can be defined clearly (Figure 2).

We assumed that when the W3 water table is shallower than −8 m, all the solute in W3 are derived from the vadose zone, thus this water accounts for the chemical weathering flux from the vadose zone (F_{v_1}; mg d^{-1}; equation (1)). In fact, as the W3 water table fluctuated in this zone, solute concentrations do increase with decreasing depth (Figure 2), implying possible water chemistry evolution in this shallow groundwater or mixing with deeper groundwater. However, the concentration changes in this interval of the saturated zone are much smaller than those through the vadose zone. This approach, thus, may estimate the maximum limit of the vadose zone flux. When the W3 water table drops below −8 m, this water represents the chemical weathering flux from the deeper saturated zone (F_{s_1}; mg d^{-1}; equation (2)). The sum of these two estimates would be the total chemical weathering flux (F_t; mg d^{-1}; equation (3)):if W3 water table >-8 m,

$$F_{v_1} = (40[Ca_{W3}] + 24.3[Mg_{W3}] + 23[Na_{W3}] + 40[K_{W3}] + 28[Si_{W3}])D \quad (1)$$

If W3 water table $<= -8$ m,

$$F_{s_1} = (40[Ca_{W3}] + 24.3[Mg_{W3}] + 23[Na_{W3}] + 40[K_{W3}] + 28[Si_{W3}])D \quad (2)$$

$$F_t = F_{v_1} + F_{s_1} \quad (3)$$

where the subscript W3 for all the constituents indicates the solute concentrations in W3 in mM, the coefficients are the molar mass of each constituent (g $mole^{-1}$), and D is the daily discharge of Elder Creek (L d^{-1}). Then, we estimated the losses of Ca (Ca_p; mg d^{-1}) and Si (Si_p; mg d^{-1}) as solid as follows:if $[Ca_{W3}] > [Ca_E]$,

$$Ca_p = 40([Ca_{W3}] - [Ca_E])D \quad (4)$$

if $[Si_{W3}] > [Si_E]$,

Table 4. Summary of Input Variables and Results of Chemical Weathering Flux Calculations

Input Variables		
log[C[a]] − log [Q[b]]		
log[Ca] = −0.116 log[Q] − 0.35 (R^2 = 0.64)	log[Mg] = −0.0978 log[Q] − 0.64 (R^2 = 0.57)	log[Na] = −0.091 log[Q] – 0.41(R^2 = 0.52)
log[K] = −0.04 log[Q] −1. 25 (R^2 = 0.1)	log[Si] = −0.0062 log[Q] −0.56 (R^2 = 0.001)	

Approach 1		Approach 2		
Filling W3 chemistry data gaps		Minimum solute concentrations in groundwater		
Solute	When W3 water table (x[d]; m) >−8 m (mM)	When W3 water table <= −8 m (mM)[e]	Solute	Well	mM
Ca	[Ca] = −0.08x − 0.109	2.03	Ca	W10	0.07
Mg	[Mg] = −0.01x + 0.06	0.3	Mg	W10	0.06
Na	[Na] = −0.02x + 0.17	0.43	Na	W10	0.17
K	[K] = −0.001x + 0.006	0.024	K	W3	0.006
Si[c]	[Si] = −0.005x − 0.33	0.26	Si[c]	W10	0.38

Results

	mm yr^{-1}		Fluxes (t km^{-2} yr^{-1})								
				Approach 1		Approach 2				Total chemical flux	
Water year	Annual rainfall	Annual runoff	Elder Creek solute flux (F_E)	Vadose zone flux (F_{V1})	Saturated zone flux (F_{S1})	Vadose zone flux (F_{V2})	Saturated zone flux (Fs_2)	Ca loss (Ca_P)	Si loss (Si_P)	$F_E + Ca_P + Si_P$	$F_T = F_{V1} + F_{S1}$
2010	1899	1332	35.5	34.8	18.2	19	16.6	14.2	1.4	51.1	53.1
2011	2107	1484	39.5	37.6	16.4	21.1	18.4	13.4	1.3	54.2	54.0
2012	1563	931	25.1	26.1	5.5	13.1	12	4.9	1.2	31.2	31.6
2013	1331	862	21.8	23.1	6.2	12.6	9.2	5.5	1.4	28.8	29.3
Mean	1725	1152	30.5	30.4	11.6	16.4	14.1	9.5	1.3	41.3	42.01

[a]Unit in mM.
[b]Unit in L d^{-1}.
[c]Si concentration in groundwater when its Ca concentration was lowest.
[d]As negative numbers indicating water table depth below the ground surface in meter.
[e]*Kim et al.* [2014].

$$Si_p = 28([\mathrm{Si_{W3}}]-[\mathrm{Si}_E])\mathrm{D} \quad (5)$$

where the subscript $_E$ for Ca and Si indicates the concentrations these constituents in Elder Creek in mM.

The second approach is to separate the solute load of the vadose zone from the deep groundwater zone by assuming all the runoff has a vadose zone component and the representative concentration for that load is the characteristic minimum values found in our multiyear surveys. This assumption may estimate the most conservative estimate for the vadose zone flux. The solute flux from the vadose zone (F_{v_2}; mg d^{-1}) can be calculated as follows:

$$F_{v_2} = \left(40[\mathrm{Ca_{min}}]+24.3[\mathrm{Mg_{min}}]+23[\mathrm{Na_{min}}]+40[\mathrm{K_{min}}]+28\left[\mathrm{Si}_{\mathrm{min}}^{\mathrm{Ca}}\right]\right)\mathrm{D} \quad (6)$$

where the subscript min for the major cations (Ca, Mg, Na, and K) indicates the minimum concentrations of each constituent in groundwater in mM, and $\mathrm{Si}_{\mathrm{min}}^{\mathrm{Ca}}$ is the Si concentration when Ca is at the lowest value in groundwater in mM (Table 4). Then, the deeper groundwater zone solute flux (F_{s_2}; mg d^{-1}) can be inferred from the differences between the Elder Creek solute flux (F_e; mg d^{-1}) and F_{v_2}:

$$F_e = (40[\mathrm{Ca}_E]+24.3[\mathrm{Mg}_E]+23[\mathrm{Na}_E]+39[\mathrm{K}_E]+28[\mathrm{Si}_E])\mathrm{D} \quad (7)$$

$$F_{s_2} = F_e - F_{v_2} \quad (8)$$

where the subscript $_E$, again indicates the concentration of each constituent in Elder Creek in mM. Then, the chemical weathering flux for the vadose zone can be quantified by the sum of F_{v_2} and Si_p and that for the deep groundwater will be the sum of F_{s_2} and Ca_p.

The annual chemical weathering fluxes for each water year (F_{V1}, F_{V2}, F_{S1}, F_{S2}, F_T, F_E, Ca_P, and Si_P) were calculated by the sum of these daily estimates and divided by the drainage area (16.8 km^2). To fill the

observational gaps, for W3, when the water table was above −-8 m, linear regressions between the W3 solute concentrations and water table depth were used while when the water table was below −8 m, the averages of solute concentrations of this deep zone were used (Table 4 and supporting information Figure S7). For Elder Creek, the power law fittings of the solute concentration-discharge relationships were used to infer the missing data for a given daily discharge (Table 4 and supporting information Figure S8).

For four water years (2010–2013), the annual rainfall and runoff averaged 1725 and 1152 mm yr^{-1}, respectively (average runoff ratio = 0.67; Table 4). The annual solute flux of Elder Creek (F_E) averaged 30.5 t km^{-2} yr^{-1} while the annual total chemical weathering flux (F_T), i.e., the sum of the calculated fluxes from the two zones followed by the first method, averaged 42.01 t km^{-2} yr^{-1}. This difference may be due to the Ca and Si precipitation. Indeed, if Ca_P and Si_P are added to F_E, the differences between F_E and F_T become insignificant (Table 4). These results indicate that if the chemical weathering fluxes for Elder Creek was estimated solely by the stream observations, the flux may be underestimated nearly by 30%. Equivalent propagation rate of weathering front computed by the total chemical weathering fluxes was 0.015 mm yr^{-1}, assuming the densities of fresh argillite and calcite are 2.65 and 2.71 g cm^{-3}, respectively. This rate is much smaller than the erosion rate in Elder Creek (up to 0.4 mm yr^{-1}) [*Fuller et al*., 2009].

Our two different approaches estimated that, on average, 43($F_{V2} + Si_p$) to 74 (F_{V1}) % of the chemical weathering fluxes (F_T) may be derived from the vadose zone. In Coos Bay, *Anderson and Dietrich* [2001] estimated that the solute fluxes from the soil layer and weathered bedrock zone were approximately the same (i.e., 50% each), which is similar to our most conservative estimates for the vadose zone flux. In their study site, due to low solute concentrations, solutes may behave conservatively; thus, solute fluxes would be equal to chemical weathering fluxes. The significant chemical weathering fluxes from the vadose zone are consistent with the critical role of the vadose zone processes in buffering solute concentrations of runoff. In both sites, the vadose zone may be highly reactive such that solute concentrations of vadose zone flow are well buffered, resulting in relatively invariant solute concentrations for a large range of discharge.

5.3. The Role of Critical Zone Structure in C-Q Relationships

Although the aforementioned studies at Coos Bay primarily focused on investigating the hydrochemical processes on a hillslope and did not include the stream which the hillslope runoff drains, they essentially demonstrated that critical zone structure controlled the concentration-discharge relationships of elements issuing from the springs at the base of the hillslope. Infiltrating waters through the highly porous, organic rich soils quickly gained solutes, leaked into an underlying fractured bedrock where a perched groundwater developed. This groundwater gained additional solute loading and as it drained off the hillslope locally exfiltrated back into the soil, and eventually formed spring heads. Small changes of solute concentrations with discharge resulted because of fast evolution in the vadose zone and the modest increase in load in the groundwater runoff.

In the vadose zone, rapid reactions such as cation exchange reactions [e.g., *Anderson et al*., 1997a; *Clow and Mast*, 2010; *Jin et al*., 2011; *Kim et al*., 2014] or dissolution of highly reactive phases (i.e., amorphous Si) [e.g., *Asano et al*., 2003] are responsible for the water chemistry evolution in this zone. Because of fast kinetics of these processes, water chemistry may reach equilibrium rapidly and remain at this equilibrium value for a long period in this zone, implying that solute concentrations and water ages may not be correlated. For example, *Asano et al*. [2003] reported that the soil water residence time varied from 10 to 50 days and was structured along the soil depth while the Si concentrations were invariant with soil depth across a hillslope in the Fudoji catchment, Japan, underlain by permeable granite. The authors postulated that the dissolution of easily dissolvable Si may rapidly increase the Si concentrations in soil water; therefore, the solute concentration becomes independent of residence time.

In the absence of overland flow, these vadose zone processes may also influence on the overall relationships between transit time and stream solute concentration because all infiltrated rain waters must pass through the vadose zone to recharge groundwater and drain to the stream. Water will further concentrate solutes via mineral dissolution in the saturated zone. The concentrations, however, may increase at a slower rate than in the vadose zone because the solute concentrations approach equilibrium levels. Furthermore, mineral compositions may differ in these two zones, which may affect kinetics and equilibrium levels of dissolution reactions. For example, in the saturated zone, the dissolution of crystalline minerals (i.e., chlorite,

albite, feldspar) may be primarily responsible for solute concentrations in this zone. In general, crystalline minerals are less soluble and dissolve much slower than amorphous phases [*Drever*, 1997; *Sposito*, 2006]. Models often employ transit time arguments to simulate the water chemistry evolution in both the vadose and saturated zones and set the maximum solute concentrations at the equilibrium values [e.g., *Maher*, 2011; *Benettin et al*., 2015]; however, such differences in the kinetics and equilibrium parameters of these two zones have rarely been accounted in these models.

Godsey et al. [2009] proposed a porosity-permeability-aperture model to explain the chemostatic behavior of streams. They assumed that the porosity, permeability, and fracture aperture exponentially increase toward the surface, which may well describe the structural variations of the critical zone. As a system wets up, the reactive surface area increases; thus, rainwater chemistry would be buffered. They further suggested that if this process is the primary control for chemostatic behavior, the exponents would be the same for weathering-derived elements (i.e., major cations and Si). *Stallard and Murphy* [2014] analyzed the C-Q relationships of five watersheds in Puerto Rico and found that the weathering-derived elements displayed similar exponents: for instance, the exponents of Quebrada Guaba in the Rio Icacos Watershed were −0.34 (Ca), −0.28 (Mg), and −0.44 (Si). The authors stated that the "near constancy of slope" in each of their watershed for these elements is evidence for the *Godsey et al*. [2009]. Our analysis here, where we document the hillslope solute evolution processes, suggest that a "constancy of slope" amongst the elements can arise for different reasons than proposed by the Godsey et al. model.

The porosity-permeability-aperture model might partially explain the solute evolution processes in the vadose zone. As the water storage in the soil or saprolite layers increases, additional reactive surfaces or exchange sites may contribute to buffer the rainwater chemistry. However, as Godsey et al. also pointed out in their paper, the compositions and stoichiometry of minerals may vary with depth. Such variations may exert strong influences on the water chemistry evolution in the critical zone, and these effects are not considered in this model. Furthermore, the Godsey et al. model does not adequately describe the water chemistry evolution in the saturated fractured/weathered bedrock zone. In this zone, water flows primarily via fractures without much interaction with the stored water (rock matrix water), implying the reactive surface area is limited to the fracture surface. As the saturated zone thickens, the reactive surface will certainly increase; however, the effect would not be as prominent as it does in the soil layer. This saturated flow via fractures in the less weathered bedrock zone should be considered in the C-Q study because it may play a key role controlling the highest solute in stream.

6. Conclusion

The C-Q relationships of Elder Creek were studied by comparing the hydrochemistry observations of the stream and hillslope source groundwater that were documented simultaneously at 1–3 days frequencies for 4 years. The hillslope groundwater was perched on the fresh bedrock boundary (5–25 m below the surface) and seasonally fluctuated by 4–6 m. The stream chemistry was compared to that of the groundwater measured at three locations (i.e., upslope, midslope, and downslope) along the hillslope. The major cations and Si of Elder Creek displayed typical chemostatic behavior. During the wet season, water vertically passes through the thick vadose zone in weathered bedrock and recharges the groundwater. The solute concentrations of this flow are controlled by the cation exchange reactions enhanced by high subsurface pCO_2 and rapid dissolution of amorphous Si in the vadose zone. When the groundwater table rises to the highly conductive fractured bedrock zone, this water drains to the stream apparently without much further water chemistry evolution. In the deeper bedrock zone, the water interacts with less weathered bedrock and further concentrates solutes, even reaching equilibrium between primary and secondary minerals and saturation with calcite under high pCO_2 (1–6%). When this groundwater emerges in the stream, CO_2 degasses and its pH increases; consequently, calcite precipitates. Altogether, our observations suggest that Elder Creek's chemostatic behavior is attributed to the relatively small concentration differences between the slow, deeper flow and rapid, shallow flow waters that are controlled in the respective critical zone structures. The differences of the Ca concentrations between the vadose zone flux and deep groundwater were much greater than those of other elements; however due to the nonconservative transition from the hillslopes to the stream, Ca in Elder Creek also displayed chemostatic patterns. At least 43% and probably closer to 74% of the solute flux from the hillslope is derived from the vadose zone. Because of Ca and Si

precipitation, the solute load derived from concentration-discharge relationships in stream observations may underestimate solute flux from the hillslope by about 30%.

Our study proposes that the critical zone structure may play a key role in manifesting C-Q relationships by regulating the availability and type of weatherable material, water transit time, and flow paths. Interplay among these properties may drive the evolution of water chemistry and control the highest and lowest solute concentrations in stream. This further implies that the C-Q relationships of a watershed will coevolve as its critical zone structure develops. Therefore, investigations of the controls for the C-Q relationships may contribute to improving our understanding of the evolution of the critical zone structure.

Acknowledgments
We would like to thank three anonymous reviewers for providing constructive comments. This study was funded by the W.M. Keck Foundation (Berkeley HydroWatch Center Award), the National Science Foundation award (NSF-OCE1049222), the Department of Energy (DE-SC000147), and NSF CZP EAR-1331940 for the Eel River Critical Zone Observatory. Hyojin Kim also acknowledges funding from the National Science Foundation (EAR 13-31726) for the Shale Hills Critical Zone Observatory. We are also grateful to the University of California Natural Reserve System for establishing the Angelo Coast Range Reserve as a protected site for our research. Todd Wood (LBNL) automated the remote sampling system and provided critical help with ICP-MS analyses. UC Berkeley Undergraduate Research Apprenticeship Program (URAP) students Michael Fong, Nolan Wong, Tim Ault, Ernesto Martinez, Robert Nicklas, and Kevin Ni assisted both in the field and in the laboratory. All the data reported in this study are available at the Eel River Critical Zone Observatory website (http://criticalzone.org/eel/).

References

Anderson, S. P., and W. E. Dietrich (2001), Chemical weathering and runoff chemistry in a steep headwater catchment, *Hydrol. Processes*, *15*(10), 1791–1815, doi:10.1002/hyp.240.

Anderson, S. P., W. E. Dietrich, R. Torres, D. R. Montgomery, and K. Loague (1997a), Concentration-discharge relationships in runoff from a steep, unchanneled catchment, *Water Resour. Res.*, *33*(1), 211–225, doi:10.1029/96WR02715.

Anderson, S. P., W. E. Dietrich, D. R. Montgomery, R. Torres, M. E. Conrad, and K. Loague (1997b), Subsurface flow paths in a steep, unchanneled catchment, *Water Resour. Res.*, *33*(12), 2637–2653, doi:10.1029/97WR02595.

Asano, Y., T. Uchida, and N. Ohte (2003), Hydrologic and geochemical influences on the dissolved silica concentration in natural water in a steep headwater catchment, *Geochim. Cosmochim. Acta*, *67*(11), 1973–1989, doi:10.1016/S0016-7037(02)01342-X.

Benettin, P., S. W. Bailey, J. L. Campbell, M. B. Green, A. Rinaldo, G. E. Likens, K. J. McGuire, and G. Botter (2015), Linking water age and solute dynamics in streamflow at the Hubbard Brook Experimental Forest, NH, USA, *Water Resour. Res.*, *51*, 9256–9272, doi:10.1002/2015WR017552.

Bluth, G. J. S., and L. R. Kump (1994), Lithologic and climatologic controls of river chemistry, *Geochim. Cosmochim. Acta*, *58*(10), 2341–2359, doi:10.1016/0016-7037(94)90015-9.

Burns, D. A., R. P. Hooper, J. J. Mcdonnell, J. Freer, C. Kendall, and K. J. Beven (1998), Base cation concentrations in subsurface flow from a forested hillslope—The role of flushing frequency, *Water Resour. Res.*, *34*(12), 3535–3544, doi:10.1029/98WR02450.

Burns, D. A., J. J. McDonnell, R. P. Hooper, N. E. Peters, J. E. Freer, C. Kendall, and K. Beven (2001), Quantifying contributions to storm runoff through end-member mixing analysis and hydrologic measurements at the Panola Mountain research watershed (Georgia, USA), *Hydrol. Processes*, *15*(10), 1903–1924, doi:10.1002/hyp.246.

Calmels, D., A. Galy, N. Hovius, M. Bickle, J. West, M.-C. Chen, and H. Chapman (2011), Contribution of deep groundwater to the weathering budget in a rapidly eroding mountain belt, Taiwan, *Earth Planet. Sci. Lett.*, *303*(1–2), 48–58, doi:10.1016/j.epsl.2010.12.032.

Clow, D. W., and M. A. Mast (2010), Mechanisms for chemostatic behavior in catchments: Implications for CO_2 consumption by mineral weathering, *Chem. Geol.*, *269*(1–2), 40–51, doi:10.1016/j.chemgeo.2009.09.014.

Drever, J. I. (1997), *The Geochemistry of Natural Waters: Surface and Groundwater Environments*, 3rd ed., Prentice-Hall, Upper Saddle River, N. J.

Fuller, T. K., L. A. Perg, J. K. Willenbring, and K. Lepper (2009), Field evidence for climate-driven changes in sediment supply leading to strath terrace formation, *Geology*, *37*(5), 467–470, doi:10.1130/G25487A.1.

Godsey, S. E., J. W. Kirchner, and D. W. Clow (2009), Concentration-discharge relationships reflect chemostatic characteristics of US catchments, *Hydrol. Processes*, *23*(13), 1844–1864, doi:10.1002/hyp.7315.

Haria, A. H., and P. Shand (2004), Evidence for deep sub-surface flow routing in forested upland Wales: Implications for contaminant transport and stream flow generation, *Hydrol. Earth Syst. Sci.*, *8*(3), 334–344, doi:10.5194/hess-8-334-2004.

Herndon, E. M., A. L. Dere, P. L. Sullivan, D. Norris, B. Reynolds, and S. L. Brantley (2015), Landscape heterogeneity drives contrasting concentration-discharge relationships in shale headwater catchments, *Hydrol. Earth Syst. Sci.*, *19*(8), 3333–3347, doi:10.5194/hess-19-3333-2015.

Jin, L., D. M. Andrews, G. H. Holmes, H. S. Lin, and S. L. Brantley (2011), Opening the "Black Box": Water chemistry reveals hydrological controls on weathering in the Susquehanna Shale Hills critical zone observatory, *Vadose Zone J.*, *10*(3), 928, doi:10.2136/vzj2010.0133.

Kennedy, V. C. (1971), Silica variation in stream water with time and discharge, *Nonequilibrium Syst. Nat. Water Chem.*, *196*, 94–130.

Kim, H., J. K. B. Bishop, T. J. Wood, and I. Y. Fung (2012), Autonomous water sampling for long-term monitoring of trace metals in remote environments, *Environ. Sci. Technol.*, *46*(20), 11,220–11,226, doi:10.1021/es3006404.

Kim, H., J. K. B. Bishop, W. E. Dietrich, and I. Y. Fung (2014), Process dominance shift in solute chemistry as revealed by long-term high-frequency water chemistry observations of groundwater flowing through weathered argillite underlying a steep forested hillslope, *Geochim. Cosmochim. Acta*, *140*, 1–19, doi:10.1016/j.gca.2014.05.011.

Kirchner, J. W., and C. Neal (2013), Universal fractal scaling in stream chemistry and its implications for solute transport and water quality trend detection, *Proc. Natl. Acad. Sci. U. S. A.*, *110*(30), 12,213–12,218, doi:10.1073/pnas.1304328110.

Kirchner, J. W., X. Feng, and C. Neal (2001), Catchment-scale advection and dispersion as a mechanism for fractal scaling in stream tracer concentrations, *J. Hydrol.*, *254*(1–4), 82–101, doi:10.1016/S0022-1694(01)00487-5.

Langenheim, V. E., R. C. Jachens, C. M. Wentworth, and R. J. Mclaughlin (2013), Previously unrecognized regional structure of the Coastal Belt of the Franciscan Complex, northern California, revealed by magnetic data, *Geosphere*, *9*(6), 1514–1529, doi:10.1130/GES00942.1.

Likens, G. E., C. T. Driscoll, D. C. Buso, T. G. Siccama, C. E. Johnson, G. M. Lovett, D. F. Ryan, T. J. Fahey, and W. A. Reiner (1994), The biogeochemistry of potassium at Hubbard Brook, *Biogeochemistry*, *25*(2), 61–125.

Lovill, S. M. (2016), *Drainage From the Critical Zone: Lithologic, Aspect, and Vegetation Controls on the Persistence and Spatial Extent of Wetted Channels During the Summer Dry Season*, 109 pp., Master of Science, University of California, Berkeley, Calif.

Luxmoore, R. J., P. M. Jardine, G. V. Wilson, J. R. Jones, and L. W. Zelazny (1990), Physical and chemical controls of preferred path flow through a forested hillslope, *Geoderma*, *46*(1–3), 139–154, doi:10.1016/0016-7061(90)90012-X.

Macinnis-Ng, C. M. O., E. E. Flores, H. Müller, and L. Schwendenmann (2012), Rainfall partitioning into throughfall and stemflow and associated nutrient fluxes: Land use impacts in a lower montane tropical region of Panama, *Biogeochemistry*, *111*(1–3), 661–676, doi:10.1007/s10533-012-9709-0.

Maher, K. (2011), The role of fluid residence time and topographic scales in determining chemical fluxes from landscapes, *Earth Planet. Sci. Lett.*, *312*(1–2), 48–58, doi:10.1016/j.epsl.2011.09.040.

Markewitz, D., E. C. Lamon, M. C. Bustamante, J. Chaves, R. O. Figueiredo, M. S. Johnson, A. Krusche, C. Neill, and J. S. O. Silva (2011), Discharge-calcium concentration relationships in streams of the Amazon and Cerrado of Brazil: Soil or land use controlled, *Biogeochemistry*, *105*(1–3), 19–35, doi:10.1007/s10533-011-9574-2.

Mast, M. A., and D. W. Clow (2000), *Environmental Characteristics and Water-Quality of Hydrologic Benchmark Network Stations in the Western United States, U.S. Geol. Surv. Circ. 1173-D*, 115 pp., U.S. Geological Survey, Reston, Va.

McDonnell, J. J. (1990), A rationale for old water discharge through macropores in a steep, humid catchment, *Water Resour. Res.*, *26*(11), 2821–2832, doi:10.1029/WR026i011p02821.

McGuire, K. J., and J. J. McDonnell (2006), A review and evaluation of catchment transit time modeling, *J. Hydrol.*, *330*(3–4), 543–563, doi:10.1016/j.jhydrol.2006.04.020.

Mclaughlin, R. J., S. D. Ellen, J. M. C. Blake, A. S. Jayko, W. P. Irwin, K. R. Aalto, G. A. Carver, and J. S. H. Clark (2000), *Geology of the Cape Mendocino, Eureka, Garberville, and Southwestern Part of the Hayfork 30 x 60 Minute Quadrangles and Adjacent Offshore Area, Northern California, with digital database*, Miscellaneous Field Studies Map MF-2336, U.S. Geological Survey, Reston, Va.

Montgomery, D. R., and W. E. Dietrich (2002), Runoff generation in a steep, soil-mantled landscape, *Water Resour. Res.*, *38*(9), 1168, doi:10.1029/2001WR000822.

Montgomery, D. R., W. E. Dietrich, R. Torres, S. P. Anderson, J. T. Heffner, and K. Loague (1997), Hydrologic response of a steep, unchanneled valley to natural and applied rainfall, *Water Resour. Res.*, *33*(1), 91–109, doi:10.1029/96WR02985.

Mulholland, P. J., G. V. Wilson, and P. M. Jardine (1990), Hydrogeochemical Response of a Forested Watershed to Storms: Effects of Preferential Flow Along Shallow and Deep Pathways, *Water Resour. Res.*, *26*(12), 3021, doi:10.1029/WR026i012p03021.

Neal, C., et al. (1997a), The occurrence of groundwater in the Lower Palaeozoic rocks of upland Central Wales, *Hydrol. Earth Syst. Sci.*, *1*(1), 3–18, doi:10.5194/hess-1-3-1997.

Neal, C., et al. (1997b), The occurrence of groundwater in the Lower Palaeozoic rocks of upland Central Wales, *Hydrol. Earth Syst. Sci.*, *1*(1), 3–18, doi:10.5194/hess-1-3-1997.

Oshun, J., W. E. Dietrich, T. E. Dawson, and I. Fung (2016), Dynamic, structured heterogeneity of water isotopes inside hillslopes, *Water Resour. Res.*, *52*, 164–189, doi:10.1002/2015WR017485.

Rempe, D. M. (2016), *Controls on Critical Zone Thickness and Hydrologic Dynamics at the Hillslope Scale*, Univ. of California, Berkeley, Calif.

Salve, R., D. M. Rempe, and W. E. Dietrich (2012), Rain, rock moisture dynamics, and the rapid response of perched groundwater in weathered, fractured argillite underlying a steep hillslope, *Water Resour. Res.*, *48*, W11528, doi:10.1029/2012WR012583.

Shand, P., A. H. Haria, C. Neal, K. J. Griffiths, D. C. Gooddy, A. J. Dixon, T. Hill, D. K. Buckley, and J. E. Cunningham (2005), Hydrochemical heterogeneity in an upland catchment: Further characterisation of the spatial, temporal and depth variations in soils, streams and groundwaters of the Plynlimon forested catchment, Wales, *Hydrol. Earth Syst. Sci. Discuss.*, *9*(6), 621–644, doi:10.5194/hess-9-621-2005.

Shanley, J. B., W. H. McDowell, and R. F. Stallard (2011), Long-term patterns and short-term dynamics of stream solutes and suspended sediment in a rapidly weathering tropical watershed, *Water Resour. Res.*, *47*, W07515, doi:10.1029/2010WR009788.

Sidle, R. C., Y. Tsuboyama, S. Noguchi, I. Hosoda, M. Fujieda, and T. Shimizu (2000), Stormflow generation in steep forested headwaters: A linked hydrogeomorphic paradigm, *Hydrol. Processes*, *14*(3), 369–385, doi:10.1002/(SICI)1099-1085(20000228)14:3<369::AID-HYP943>3.0.CO;2-P.

Sposito, G. (2006), *The Chemistry of Soils*, 2nd ed., Oxford Univ. Press, New York.

Stallard, R. F., and S. F. Murphy (2014), A unified assessment of hydrologic and biogeochemical responses in research watersheds in Eastern Puerto Rico using runoff-concentration relations, *Aquat. Geochem.*, *20*(2–3), 115–139, doi:10.1007/s10498-013-9216-5.

Tetzlaff, D., J. Seibert, K. J. McGuire, H. Laudon, D. A. Burns, S. M. Dunn, and C. Soulsby (2009), How does landscape structure influence catchment transit time across different geomorphic provinces?, *Hydrol. Processes*, *23*(6), 945–953, doi:10.1002/hyp.7240.

Tobon, C., J. A. N. Sevink, and J. M. Verstraten (2004), Solute fluxes in throughfall and stemflow in four forest ecosystems in Northwest Amazonia, *Biogeochemistry*, *70*(1), 1–25.

Torres, R., W. E. Dietrich, D. R. Montgomery, S. P. Anderson, and K. Loague (1998), Unsaturated zone processes and the hydrologic response of a steep, unchanneled catchment, *Water Resour. Res.*, *34*(8), 1865, doi:10.1029/98WR01140.

Tromp-van Meerveld, H. J., and J. J. McDonnell (2006), Threshold relations in subsurface stormflow: 1. A 147-storm analysis of the Panola hillslope, *Water Resour. Res.*, *42*, W02410, doi:10.1029/2004WR003778.

Tromp-van Meerveld, H. J., N. E. Peters, and J. J. McDonnell (2007), Effect of bedrock permeability on subsurface stormflow and the water balance of a trenched hillslope at the Panola Mountain Research Watershed, Georgia, USA, *Hydrol. Processes*, *21*(6), 750–769, doi:10.1002/hyp.6265.

U.S. Environmental Protection Agency (1996), *Method 1669 Sampling Ambient Water for Trace Metals at EPA Water Quality Criteria Levels*, United State Environmental Protection Agency Office of Water Engineering and Analysis Division, Washington, D. C.

Uchida, T., Y. Asano, N. Ohte, and T. Mizuyama (2003), Seepage area and rate of bedrock groundwater discharge at a granitic unchanneled hillslope, *Water Resour. Res.*, *39*(1), 1018, doi:10.1029/2002WR001298.

Uchida, T., I. Tromp-Van Meerveld, and J. J. McDonnell (2005), The role of lateral pipe flow in hillslope runoff response: An intercomparison of non-linear hillslope response, *J. Hydrol.*, *311*(1–4), 117–133, doi:10.1016/j.jhydrol.2005.01.012.

Uchida, T., J. J. McDonnell, and Y. Asano (2006), Functional intercomparison of hillslopes and small catchments by examining water source, flowpath and mean residence time, *J. Hydrol.*, *327*(3–4), 627–642, doi:10.1016/j.jhydrol.2006.02.037.

Underwood, M. B., and S. B. Bachman (1986), Sandstone petrofacies of the Yagar complex and the Franciscan coastal belt, Paleogene of northern California, *Geol. Soc. Am. Bull.*, *97*(7), 809–817, doi:10.1130/0016-7606(1986)97<809:SPOTYC>2.0.CO;2.

White, A. F., and A. E. Blum (1995), Effects of climate on chemical weathering in watersheds, *Geochim. Cosmochim. Acta*, *59*(9), 1729–1747, doi:10.1016/0016-7037(95)00078-E.